

ROUNDING ERROR ANALYSIS OF MIXED PRECISION BLOCK HOUSEHOLDER QR ALGORITHMS

L. MINAH YANG, ALYSON FOX, AND GEOFFREY SANDERS

Abstract. Although mixed precision arithmetic has recently garnered interest for training dense neural networks, many other applications could benefit from the speed-ups and lower storage if applied appropriately. The growing interest in employing mixed precision computations motivates the need for rounding error analysis that properly handles behavior from mixed precision arithmetic. We develop mixed precision variants of existing Householder QR algorithms and show error analyses supported by numerical experiments.

1. Introduction. The accuracy of a numerical algorithm depends on several factors, including numerical stability and well-conditionedness of the problem, both of which may be sensitive to rounding errors, the difference between exact and finite-precision arithmetic. Low precision floats use fewer bits than high precision floats to represent the real numbers and naturally incur larger rounding errors. Therefore, error attributed to round-off may have a larger influence over the total error when using low precision, and some standard algorithms may yield insufficient accuracy when using low precision storage and arithmetic. However, many applications exist that would benefit from the use of low precision arithmetic and storage that are less sensitive to floating-point round off error, such as clustering or ranking graph algorithms [24] or training dense neural networks [20].

Many computing applications today require solutions quickly and often under low size, weight, and power constraints, such as in sensor formation, where low precision computation offers the ability to solve many problems with improvement in all four parameters. Utilizing mixed precision, one can achieve similar quality of computation as high-precision and still achieve speed, size, weight, and power constraint improvements. There have been several recent demonstrations of computing using IEEE half precision (fp16) achieving around half an order to an order of magnitude improvement of these categories in comparison to single and double precision (fp32, fp64). Trivially, the size and weight of memory required for a specific problem is $4\times$. Additionally, there exist demonstrations that the power consumption improvement is similar [11]. Modern accelerators (e.g., GPUs, Knights Landing, or Xeon Phi) are able to achieve this factor or better speedup improvements. Several examples include: (i) $2\text{--}4\times$ speedup in solving dense large linear equations [13, 14], (ii) $12\times$ speedup in training dense neural networks, and (iii) $1.2\text{--}10\times$ speedup in small batched dense matrix multiplication [1] (up to $26\times$ for batches of tiny matrices). Training deep artificial neural networks by employing lower precision arithmetic to various tasks such as multiplication [7] and storage [8] can easily be implemented on GPUs and are a common practice in some data science applications.

The low precision computing environments that we consider are *mixed precision* settings, which are designed to imitate those of new GPUs that employ multiple precision types for certain tasks. For example, Tesla V100's TensorCores perform block Fused Multiply Add operations (bFMAs), where matrix products of fp16 input data can be computed up to $16\times$ than that of fp64. The existing rounding error analyses are built within what we call a *uniform precision* setting, which is the assumption that all arithmetic operations and storage are performed via the same precision. In this work, we develop mixed precision variants of existing Householder (HH) QR factorization algorithms and perform mixed precision error analysis.

This work was performed under the auspices of the U.S. Department of Energy by Lawrence Livermore National Laboratory under Contract DE-AC52-07NA27344 and was supported by the LLNL-LDRD Program under Project No. 17-SI-004, LLNL-JRNL-795525-DRAFT.

41 This work focuses on analyzing a few algorithms that use fp16/fp32 as the low/high precision
 42 types, but the error analysis can be easily modified for different floating point types (such as
 43 bfloat16 in [23]). The standard HH QR algorithm and its block variants that partition the columns
 44 (level-3 BLAS variant, see [12, 15]) and those that partition the columns (communication-avoiding
 45 algorithms of [10]) are presented in section 3, then modified to support bFMAs and an ad hoc mixed
 46 precision setting that mimics NVIDIA TensorCores in section 4. Our key findings are that mixed
 47 precision error analyses produce tighter error bounds as supported by experiments in section 5,
 48 algorithms that utilize level-3 BLAS operations can easily be modified to incorporate TensorCore
 49 bFMAs, and a row partition block algorithm operates more robustly in mixed precision than non-
 50 block techniques in certain regimes.

51 **2. Background: Build up to rounding error analysis for inner products.** In this
 52 section, we introduce the basic motivations and tools for mixed precision rounding error analysis
 53 needed for the *QR factorization*. A matrix $\mathbf{A} \in \mathbb{R}^{m \times n}$ for $m \geq n$ can be written as

$$54 \quad \mathbf{A} = \mathbf{QR} = [\mathbf{Q}_1 \quad \mathbf{Q}_2] \begin{bmatrix} \mathbf{R}_1 \\ \mathbf{0}_{m-n \times n} \end{bmatrix} = \mathbf{Q}_1 \mathbf{R}_1,$$

55 where an orthogonal $\mathbf{Q} \in \mathbb{R}^{m \times m}$ and an upper trapezoidal \mathbf{R} form a *full* QR factorization, and
 56 $\mathbf{Q}_1 \in \mathbb{R}^{m \times n}$, $\mathbf{R}_1 \in \mathbb{R}^{n \times n}$ form a *thin* QR factorization. If \mathbf{A} is full rank then the columns of \mathbf{Q}_1 are
 57 orthonormal and \mathbf{R}_1 is upper triangular. In many applications, computing the *thin* decomposition
 58 requires less computation and is sufficient in performance. While important definitions are stated
 59 explicitly in the text, Table 1 serves to establish basic notation.

| Symbol | Definition | Section |
|--|--|---------|
| $\mathbf{x}, \mathbf{A}, \mathbf{x} , \mathbf{A} $ | Vector, matrix, and absolute value of each component | 2 |
| $\ \mathbf{x}\ _p, \ \mathbf{A}\ _p$ | Vector, operator p -norms for $p = 2$, and Frobenius norm when $p = F$. | 2 |
| $\mathbf{x}[i], \mathbf{A}[i, j], :$ | i^{th} element of \mathbf{x} , i^{th} row and j^{th} column element of \mathbf{A} , all indices | 2 |
| $\mathbf{X}_{m \times n}, \mathbf{X}_n$ | m -by- n or n -by- n matrices for \mathbf{X} in $\{\mathbf{0}, \mathbf{I}\}$, $\mathbf{I}_{m \times n} = [\mathbf{I}_n \quad \mathbf{0}_{n \times (m-n)}]^\top$ | 1 |
| $\hat{\mathbf{e}}_i$ | i^{th} cardinal vector | 1 |
| \mathbf{Q}, \mathbf{R} | Factors resulting from Householder (HH) QR factorization algorithms | 2 |
| $\mathbf{P}_v, \mathbf{P}_i$ | HH transformation corresponding to \mathbf{v} , i^{th} HH transformation in HQR | 3 |
| $\mathbf{X}, \mathbf{W}, \mathbf{Y}$ | WY representation of successive HH transformations, $\mathbf{X} = \mathbf{I} - \mathbf{WY}^\top$ | |
| $\text{fl}(\mathbf{x}), \hat{\mathbf{x}}$ | Quantity \mathbf{x} calculated from floating point operations | 2 |
| μ, η | mantissa, exponent bits of a floating point number | 2 |
| $b_q, t_q, u^{(q)}$ | base, precision, unit round-off for precision q , $u^{(q)} := \frac{1}{2}b_q^{1-t_q}$ | 2 |
| $\delta^{(q)}$ | Quantity bounded by: $ \delta^{(q)} < u^{(q)}$ | 2 |
| $\gamma_k^{(q)}, \theta_k^{(q)}$ | $\frac{ku^{(q)}}{1-ku^{(q)}}$, Quantity bounded by: $ \theta_k^{(q)} \leq \tilde{\gamma}_k^{(q)}$ | 2 |
| $\tilde{\gamma}_k^{(q)}, \tilde{\theta}_k^{(q)}$ | $\frac{cku^{(q)}}{1-cku^{(q)}}$ for small integer $c > 0$, Quantity bounded by: $ \theta_k^{(q)} \leq \gamma_k^{(q)}$ | 2 |

TABLE 1
Basic definitions and where they first appear.

60 **2.1. Basic rounding error analysis of floating point operations.** We use and analyze
 61 the IEEE 754 Standard floating point number systems, shown in Table 2. Let $\mathbb{F} \subset \mathbb{R}$ denote the
 62 space of some floating point number system with base $b \in \mathbb{N}$, precision $t \in \mathbb{N}$, significand $\mu \in \mathbb{N}$,
 63 and exponent range $[\eta_{\min}, \eta_{\max}] \subset \mathbb{Z}$. Then every element y in \mathbb{F} can be written as

$$64 \quad (2.1) \quad y = \pm \mu \times b^{\eta-t},$$

where μ is any integer in $[0, b^t - 1]$ and η is an integer in $[\eta_{\min}, \eta_{\max}]$. Although operations we use on \mathbb{R} cannot be replicated exactly due to the finite cardinality of \mathbb{F} , we can still approximate the accuracy of analogous floating point operations (FLOPs). We adopt the rounding error analysis tools described in [15], which allow a relatively simple framework for formulating error bounds for complex linear algebra operations. An analysis of FLOPs (see Theorem 2.2 [15]) shows that the relative error is controlled by the unit round-off, $u := \frac{1}{2}b^{1-t}$ in uniform precision settings. In mixed precision settings we denote the higher precision unit round-off with $u^{(h)}$ (h for high) and the lower precision unit round-off with $u^{(l)}$ (l for low).

| Name | b | t | # of exponent bits | η_{\min} | η_{\max} | unit round-off u |
|-----------------------|-----|-----|--------------------|---------------|---------------|--------------------|
| fp16 (IEEE754 half) | 2 | 11 | 5 | -15 | 16 | 4.883e-04 |
| fp32 (IEEE754 single) | 2 | 24 | 8 | -127 | 128 | 5.960e-08 |
| fp64 (IEEE754 double) | 2 | 53 | 11 | -1023 | 1024 | 1.110e-16 |

TABLE 2
IEEE754 formats and their primary attributes.

Let ‘op’ be any basic operation from the set $\text{OP} = \{+, -, \times, \div\}$ and let $x, y \in \mathbb{R}$. The true value $(x \text{ op } y)$ lies in \mathbb{R} , and it is rounded using some conversion to a floating point number, $\text{fl}(x \text{ op } y)$, admitting a rounding error. The IEEE 754 Standard requires *correct rounding*, which rounds the exact solution $(x \text{ op } y)$ to the closest floating point number and, in case of a tie, to the floating point number that has a mantissa ending in an even number. *Correct rounding* gives us an assumption for the error model where a single basic floating point operation yields a relative error, δ , bounded in the following sense:

$$(2.2) \quad \text{fl}(x \text{ op } y) = (1 + \delta)(x \text{ op } y), \quad |\delta| \leq u, \quad \text{op} \in \{+, -, \times, \div\}.$$

We use (2.2) as a building block in accumulating errors from successive FLOPs. Successive operations introduce multiple rounding error terms, and keeping track of all errors is challenging. Lemma 2.1 introduces a convenient and elegant bound that simplifies accumulation of rounding error.

LEMMA 2.1 (Lemma 3.1 [15]). Let $|\delta_i| < u$, $\rho_i = \pm 1$ for $i = 1 : k$, and $ku < 1$. Then,

$$(2.3) \quad \prod_{i=1}^k (1 + \delta_i)^{\rho_i} = 1 + \theta_k, \quad \text{where } |\theta_k| \leq \frac{ku}{1 - ku} =: \gamma_k.$$

Additionally, we define $\tilde{\theta}_k$ that satisfies $|\tilde{\theta}_k| \leq \tilde{\gamma}_k$, where $\tilde{\gamma}_k = \frac{cku}{1 - cku}$ for a small integer, $c > 0$.

In other words, θ_k represents the accumulation of rounding errors from k successive operations, and it is bounded by γ_k . In more complicated routines shown in later sections, we use the tilde notation ($\tilde{\gamma}_k$) to permit only keeping track of the leading order error terms. Applying this lemma to the computation of $x + y + z$, where $x, y, z \in \mathbb{R}$, results in

$$(2.4) \quad \text{fl}(x + y + z) = (1 + \delta')((1 + \delta)(x + y) + z) = (1 + \theta_2)(x + y) + (1 + \theta_1)z,$$

where $|\delta|, |\delta'| < u$. Since $|\theta_1| \leq \gamma_1 < \gamma_2$, we can further simplify (2.4) to

$$(2.5) \quad \text{fl}(x + y + z) = (1 + \theta'_2)(x + y + z), \quad \text{where } |\theta'_2| \leq \gamma_2,$$

at the cost of a slightly larger upper bound. Note that both $|\theta_2|, |\theta'_2|$ are bounded above by γ_2 . Typically, error bounds formed in the fashion of (2.5) are converted to relative errors in order to

put the error magnitudes in perspective. The relative error bound for our example is

$$|(x + y + z) - \text{fl}(x + y + z)| \leq \gamma_2 |x + y + z|, \quad x + y + z \neq 0.$$

Although Lemma 2.1 requires $ku < 1$, we actually need $ku < \frac{1}{2}$ to maintain a meaningful relative error bound as this assumption implies $\gamma_k < 1$ and guarantees a relative error below 100%. Since higher precision types have smaller unit round-offs, they can tolerate more successive FLOPs than lower precision floating types before reaching $\gamma_m = 1$. For example, the IEEE types introduced in Table 2 meet this requirement at $1/2 = 2^{10} u(\text{fp16}) = 2^{23} u(\text{fp32}) = 2^{52} u(\text{fp64})$. Thus, accumulated rounding errors in lower precision types can lead to an instability with fewer operations in comparison to higher precision types and prompts us to evaluate whether existing algorithms can be naively adapted for mixed precision arithmetic.

2.2. Rounding Error Example for the Inner Product. We now consider computing the inner product of two vectors to clearly illustrate how this situation restricts rounding error analysis in fp16. An error bound for an inner product of m -length vectors is

$$(2.6) \quad |\mathbf{x}^\top \mathbf{y} - \text{fl}(\mathbf{x}^\top \mathbf{y})| \leq \gamma_m |\mathbf{x}|^\top |\mathbf{y}|, \quad \mathbf{x}, \mathbf{y} \in \mathbb{R}^m$$

as shown in [15]. Since vectors of length m accumulate rounding errors that are bounded by γ_m , dot products of vectors computed in fp16 already face a 100% relative error bound when $m = 1024$.

A simple numerical experiment shows that the standard deterministic error bound is too pessimistic and cannot be practically used to approximate rounding error for half-precision arithmetic. In this experiment, we generated 2 million random fp16 vectors of length 1024 from two random distributions: the standard normal distribution, $N(0, 1)$, and the uniform distribution over $(0, 1)$. Half precision arithmetic was simulated by calling `alg. 1`, which was proven to be a faithful simulation in [17], for every FLOP (multiplication and addition for the dot product). The relative error in this experiment is formulated as the LHS in Equation 2.6 divided by $|\mathbf{x}|^\top |\mathbf{y}|$ and all operations outside of calculating $\text{fl}(\mathbf{x}^\top \mathbf{y})$ are executed by casting up to fp64 and using fp64 arithmetic. Table 3 shows some statistics from computing the relative error for simulated fp16 dot products.

| Random Distribution | Average | Stan. Dev. | Maximum |
|---------------------|-----------|------------|-----------|
| Standard normal | 1.621e-04 | 1.635e-04 | 3.204e-03 |
| Uniform (0, 1) | 6.904e-03 | 3.265e-03 | 2.447e-02 |

TABLE 3

Forward error statistics from experiment of dot products computed in simulated half precision.

We see that the inner products of vectors sampled from the standard normal distribution have backward relative errors that do not deviate much from the unit round-off ($\mathcal{O}(1\text{e-}4)$), whereas the vectors sampled from the uniform distribution tend to accumulate larger errors on average ($\mathcal{O}(1\text{e-}3)$). Even so, the theoretical upper error bound of 100% is far too pessimistic as the maximum relative error does not even meet 2% in this experiment. Recent work in developing probabilistic bounds on rounding errors of floating point operations (see [16, 19]) have shown that the inner product relative backward error for the conditions used for this experiment is bounded by $5.466\text{e-}2$ with probability 0.99.

Most importantly, we need error analysis that allows flexibility in precision in order to better our understanding of the impact of rounding errors on computations done on emerging hardware

Algorithm 1: $\mathbf{z}^{(\text{fp16})} = \text{simHalf}(f, \mathbf{x}^{(\text{fp16})}, \mathbf{y}^{(\text{fp16})})$. Given fp16 input variables \mathbf{x}, \mathbf{y} , perform function $f \in \text{OP} \cup \{\text{dot_product}\}$ in simulated fp16 arithmetic.

| | |
|---|--|
| Input: $\mathbf{x}^{(\text{fp16})}, \mathbf{y}^{(\text{fp16})}, f$ 1 $[\mathbf{x}^{(\text{fp32})}, \mathbf{y}^{(\text{fp32})}] \leftarrow \text{castup}([\mathbf{x}^{(\text{fp16})}, \mathbf{y}^{(\text{fp16})}])$ 2 $\mathbf{z}^{(\text{fp32})} \leftarrow \text{fl}(f(\mathbf{x}^{(\text{fp32})}, \mathbf{y}^{(\text{fp32})}))$ 3 $\mathbf{z}^{(\text{fp16})} \leftarrow \text{castdown}(\mathbf{z}^{(\text{fp32})})$ 4 return $\mathbf{z}^{(\text{fp16})}$ | Output: $\mathbf{z}^{(\text{fp16})} = \text{fl}_{\text{fp16}}(f(\mathbf{x}^{(\text{fp16})}, \mathbf{y}^{(\text{fp16})}))$ // Convert input vars to fp32. // Perform fp32 arithmetic. // Convert result to fp16. |
|---|--|

(i.e. GPUs) that support mixed precision. We start by introducing some additional rules from [15] that build on Lemma 2.1 in Lemma 2.2. These rules summarize how to accumulate errors represented by θ 's and γ 's in a *uniform precision* setting.

LEMMA 2.2. *For any positive integer k , let θ_k denote a quantity bounded according to $|\theta_k| \leq \frac{ku}{1-ku} =: \gamma_k$. The following relations hold for positive integers j, n and nonnegative integer k . Arithmetic operations between bounded terms, θ_k 's, are:*

$$(2.7) \quad (1 + \theta_k)(1 + \theta_j) = (1 + \theta_{k+j}) \quad \text{and} \quad \frac{1 + \theta_k}{1 + \theta_j} = \begin{cases} 1 + \theta_{k+j}, & j \leq k \\ 1 + \theta_{k+2j}, & j > k \end{cases}.$$

If $\max_{(j,k)} u \leq \frac{1}{2}$ and $n \leq \frac{1}{uk}$, the operations on the bounds, γ 's, are:

$$\begin{aligned} \gamma_k \gamma_j &\leq \gamma_{\min(k,j)}, & n \gamma_k &\leq \gamma_{nk}, \\ \gamma_k + u &\leq \gamma_{k+1}, & \gamma_k + \gamma_j + \gamma_k \gamma_j &\leq \gamma_{k+j}. \end{aligned}$$

Note that all the rules hold when replaced by $\tilde{\gamma}$'s, but result in looser bounds.

We define two mixed precision settings that we use in section 4. In subsection 4.1, we present the block Fused Multiply-Add (bFMA) of NVIDIA's TensorCore (TC) technology, which computes matrix-matrix multiply and accumulate for 4-by-4 blocks, and incorporate it into algs. 5 and 6. Here, we introduce an ad hoc mixed precision setting (MP Setting) which we use in subsection 4.2. This is explicitly defined in MP Setting 2.3 and is a level-2 BLAS variant of the TC bFMA. Both mixed precision settings define how inner products are computed although the bFMA is only applicable to inner products within matrix products and uses fp16 and fp32 whereas our ad hoc mixed precision setting is applicable to all inner products with any two precision types.

Although our analysis concerns accuracy and stability and leaves out timing results of various hardwares, we add a general timing statement to MP Setting 2.3 that is analogous to that of TC: the mixed precision FMA inner product performs at least 2 times faster than the inner product in the higher precision. Note that TCs perform matrix-matrix multiply and accumulate up to 8 times faster than fp32, and up to 16 times faster than fp64 (see), and our ad hoc timing assumption is in conservative in comparison. Nonetheless, this gives a vague insight into the trade-offs between speediness and accuracy from some mixed precision computations.

The full precision multiplication in Assumption 2.3 is exact when the low precision type is fp16 and the high precision type of fp32 due to their precisions and exponent ranges. As a quick proof, consider $x^{(\text{fp16})} = \pm \mu_x 2^{\eta_x - 11}$, $y^{(\text{fp16})} = \pm \mu_y 2^{\eta_y - 11}$ where $\mu_x, \mu_y \in [0, 2^{11} - 1]$ and $\eta_x, \eta_y \in [-15, 16]$, and note that the significand and exponent ranges for fp32 are $[0, 2^{24} - 1]$ and $[-127, 128]$. Then

161 the product in full precision is

$$162 \quad x^{(\text{fp16})}y^{(\text{fp16})} = \pm\mu_x\mu_y2^{\eta_x+\eta_y+2-24},$$

163 where $\mu_x\mu_y \in [0, (2^{11} - 1)^2] \subseteq [0, 2^{24} - 1]$ and $\eta_x + \eta_y + 2 \in [-28, 34] \subseteq [-127, 128]$, and therefore
 164 is exact. Thus, the summation and the final cast down operations are the only sources of rounding
 165 error in this inner product scheme.

166 **MP SETTING 2.3.** *Let l and h each denote low and high precision types with unit round-off*
 167 *values $u^{(l)}$ and $u^{(h)}$, where $1 \gg u^{(l)} \gg u^{(h)} > 0$. Consider an FMA operation for inner products*
 168 *that take vectors stored in precision l , compute products in full precision, and sum the products in*
 169 *precision h . Finally, the result is then cast back down to precision l . Furthermore, we expect this*
 170 *procedure to be approximately twice as fast as if it were done entirely in the higher precision, and*
 171 *about the same as if it were done entirely in the lower precision.*

172 We now analyze the rounding error for the inner product scheme described in [MP Setting 2.3](#) and
 173 hypothesize that the guaranteed accuracy for this mixed precision inner product should be better
 174 than that of the low precision inner product and worse than that of the high precision inner product.
 175 Let $\mathbf{x}^{(l)}, \mathbf{y}^{(l)}$ be m -length vectors stored in a low precision type (\mathbb{F}_l^m), s_k be the exact k^{th} partial
 176 sum, and \hat{s}_k be s_k computed with FLOPs. Then the first three partial sums are,

$$177 \quad \hat{s}_1 = \text{fl}(\mathbf{x}[1]\mathbf{y}[1]) = \mathbf{x}[1]\mathbf{y}[1], \quad \hat{s}_2 = \text{fl}(\hat{s}_1 + \mathbf{x}[2]\mathbf{y}[2]) = (\mathbf{x}[1]\mathbf{y}[1] + \mathbf{x}[2]\mathbf{y}[2]) (1 + \delta_1^{(h)}),$$

$$178 \quad \hat{s}_3 = \text{fl}(\hat{s}_2 + \mathbf{x}[3]\mathbf{y}[3]) = \left[(\mathbf{x}[1]\mathbf{y}[1] + \mathbf{x}[2]\mathbf{y}[2]) (1 + \delta_1^{(h)}) + \mathbf{x}[3]\mathbf{y}[3] \right] (1 + \delta_2^{(h)}).$$

180 We see a pattern emerging. The error for an m -length vector dot product is then

$$181 \quad (2.8) \quad \hat{s}_m = (\mathbf{x}[1]\mathbf{y}[1] + \mathbf{x}[2]\mathbf{y}[2]) \prod_{k=1}^{m-1} (1 + \delta_k^{(h)}) + \sum_{i=3}^m \mathbf{x}[i]\mathbf{y}[i] \left(\prod_{k=i-1}^{m-1} (1 + \delta_k^{(h)}) \right).$$

182 Using Lemma 2.1, we further simplify and form componentwise backward errors with

$$183 \quad (2.9) \quad \text{fl}(\mathbf{x}^\top \mathbf{y}) = (\mathbf{x} + \Delta \mathbf{x})^\top \mathbf{y} = \mathbf{x}^\top (\mathbf{y} + \Delta \mathbf{y}) \quad \text{for } |\Delta \mathbf{x}| \leq \gamma_{m-1}^{(h)} |\mathbf{x}|, \quad |\Delta \mathbf{y}| \leq \gamma_{m-1}^{(h)} |\mathbf{y}|.$$

184 Casting down to \mathbb{F}_l without underflow or overflow results in backward errors,

$$185 \quad (2.10) \quad \text{castdown}(\text{fl}(\mathbf{x}^\top \mathbf{y})) = (\mathbf{x} + \Delta \mathbf{x} + \tilde{\Delta} \mathbf{x})^\top \mathbf{y} = \mathbf{x}^\top (\mathbf{y} + \Delta \mathbf{y} + \tilde{\Delta} \mathbf{y}),$$

186 where $|\Delta \mathbf{x} + \tilde{\Delta} \mathbf{x}| \leq ((1 + u^{(l)})(1 + \gamma_{m-1}^{(h)}) - 1) |\mathbf{x}|$ and $|\Delta \mathbf{y} + \tilde{\Delta} \mathbf{y}| \leq ((1 + u^{(l)})(1 + \gamma_{m-1}^{(h)}) - 1) |\mathbf{y}|$.
 187 Our hypothesis is indeed true since,

$$188 \quad \gamma_m^{(h)} < u^{(l)} + \gamma_{m-1}^{(h)} + u^{(l)} \gamma_{m-1}^{(h)} < \gamma_m^{(l)},$$

189 where the lower and upper bounds are derived from the uniform precision error bound in (2.6).
 190 Equation (2.10) shows us that the two larger error terms are from the higher precision summation,
 191 $\gamma_{m-1}^{(h)}$, and the cast down operation, $u^{(l)}$. We can measure the impact of the cast down step relative
 192 to the length of the vector, m , and the disparity in the two precisions, $M_{l,h} := u^{(l)}/u^{(h)}$, since these
 193 two factors determine which one of $u^{(l)}$ and $mu^{(h)}$ is the leading order term. We consider 3 cases.
 194 **Case 1:** ($m \ll M_{l,h}$) The leading order term is $u^{(l)}$. The mixed precision inner product has a
 195 smaller worst case error bound than the bound of the low precision inner product ($mu^{(l)}$) with no

apparent improvements in speed. On the other hand, $u^{(l)}$ is a larger upper bound than that of the high precision inner product ($mu^{(h)} = \frac{m}{M_{l,h}}u^{(l)}$), although it was computed approximately twice as fast. It is likely that this factor of $M_{l,h}/m$ increase in the worst case error bound is unwanted even when considering the speed-up.

Case 2: ($m = M_{l,h}$) Both terms are now leading order. This is still an improvement in comparison to the lower precision arithmetic as the error bound is reduced from $mu^{(l)}$ to $2u^{(l)}$. Comparing this to the high precision inner product shows that the error bound has doubled from $mu^{(h)}$ to $2mu^{(h)}$, but gained a factor of 2 in speed instead. One can argue that the loss in accuracy guarantee and the improvement in speed cancel each other out especially if $2mu^{(h)} \ll 1$ or if the speed-up greatly exceeds a factor of 2.

Case 3: ($m \gg M_{l,h}$) Now $\gamma_{m-1}^{(h)}$ is the leading order term. As in the above two cases, this is an improvement in the context of the low precision accuracy since the error has been reduced from $\gamma_m^{(l)}$ to $\gamma_{m/M_{l,h}}^{(l)} \equiv \gamma_m^{(h)}$. Since $u^{(l)} = M_{l,h}u^{(h)} \ll mu^{(h)}$, the mixed precision error bound has the same order as the error bound from carrying the computation out in the higher precision. Therefore, we can expect about the same level of accuracy but a factor of 2 or greater reduction in speed when compared to the higher precision.

While the above cases establish 3 regimes of trade-offs between accuracy and speed in mixed precision computing, the remainder of this paper focuses only on accuracy and does not consider the impact of mixed precision computations on speed. Finally, we present alternative representations of the error bound in (2.10),

$$(1 + u^{(l)})(1 + \gamma_{m-1}^{(h)}) - 1 \leq \gamma_{M_{l,h}+m-1}^{(h)} = \gamma_{1+(m-1)/M_{l,h}}^{(l)}, \quad M_{l,h} = u^{(l)}/u^{(h)},$$

$$(1 + u^{(l)})(1 + \gamma_{m-1}^{(h)}) - 1 \leq u^{(l)} + \gamma_{m-1}^{(h)} + \min\{u^{(l)}, \gamma_{m-1}^{(h)}\}, \quad \gamma_{m-1}^{(h)} < 1,$$

where the rules from Lemma 2.2 were directly applied. Both alternative bounds are only slightly larger than the original bound shown on the LHS and remain in the same order. The first is useful when comparing against the low or the high precision, whereas the second keeps track of the error bounds in both precisions. We summarize these ways of combining γ terms of different precisions in Lemma 2.4,

LEMMA 2.4. *For any nonnegative integers k_l, k_h and some precision q defined with respect to the unit round-off, $u^{(q)}$, define $\gamma_k^{(q)} := \frac{ku^{(q)}}{1-ku^{(q)}}$. Consider a low precision and a high precision where $1 \gg u^{(l)} \gg u^{(h)} > 0$, and k_l, k_h that satisfy $\max\{\gamma_{k_h}^{(h)}, \gamma_{k_l}^{(l)}\} < 1/2$. Then the following rules help us accumulate γ 's of different precisions,*

$$(2.11) \quad \gamma_{k_h}^{(h)} \gamma_{k_l}^{(l)} \leq \min\{\gamma_{k_h}^{(h)}, \gamma_{k_l}^{(l)}\},$$

$$(2.12) \quad (1 + \tilde{\gamma}_{k_l}^{(l)})(1 + \tilde{\gamma}_{k_h}^{(h)}) - 1 = \tilde{\gamma}_{k_l}^{(l)} + \tilde{\gamma}_{k_h}^{(h)}.$$

Note that (2.12) drops the term $\tilde{\gamma}_{k_l}^{(l)} \tilde{\gamma}_{k_h}^{(h)}$ since both $\tilde{\gamma}_{k_l}^{(l)}$ and $\tilde{\gamma}_{k_h}^{(h)}$ are larger than their product and this product can be swept under the small integer $c > 0$ assumption implicitly included in the tilde notation. Equations (2.9) and (2.10) are crucial for our analysis in section 4 since the two mixed precision settings add `castdown` operations at different parts of the HQR algorithms we consider. In general, error bounds in the fashion of (2.9) can be used before the cast down operations and the action of the cast down is best represented by error bounds similar to (2.10).

We have demonstrated a need for rounding error analysis that is accurate for mixed precision procedures and analyzed the inner product in an ad hoc mixed precision inner product that mimics

the TensorCore bFMA. We will use this to analyze various Householder (HH) QR factorization algorithms. Algorithms and the general framework for the standard rounding error analysis for these algorithms are introduced in [section 3](#), and both are modified to meet different mixed precision assumptions in [section 4](#).

3. Algorithms and existing round-off error analyses. We introduce the Householder QR factorization algorithm (HQR) in [subsection 3.1](#) and two block variants that use HQR within the block in [subsections 3.2](#) and [3.3](#). The blocked HQR (BQR) in [subsection 3.2](#) partitions the columns of the target matrix and is a well-known algorithm that uses the WY representation of [\[5\]](#) that utilizes mainly level-3 BLAS operations. In contrast, the Tall-and-Skinny QR (TSQR) in [subsection 3.3](#) partitions the rows and takes a communication-avoiding divide-and-conquer approach that can be easily parallelized (see [\[9\]](#)). We present the standard rounding error analysis of these algorithms which will be tweaked for various mixed precision assumptions in [section 4](#).

3.1. Householder QR (HQR). The HQR algorithm uses HH transformations to zero out elements below the diagonal of a matrix (see [\[18\]](#)). We present this as zeroing out all but the first element of some vector, $\mathbf{x} \in \mathbb{R}^m$.

LEMMA 3.1. *Given vector $\mathbf{x} \in \mathbb{R}^m$, there exist a HH vector, \mathbf{v} , and a HH constant, β , that define the HH transformation matrix, $\mathbf{P}_{\mathbf{v}} := \mathbf{I}_m - \beta \mathbf{v} \mathbf{v}^\top$, such that $\mathbf{P}_{\mathbf{v}}$ zeros out \mathbf{x} below the first element. The HH vector and constant are defined via*

$$(3.1) \quad \sigma = -\text{sign}(\mathbf{x}[1]) \|\mathbf{x}\|_2, \quad \mathbf{v} = \mathbf{x} - \sigma \hat{\mathbf{e}}_1, \quad \text{and} \quad \beta = \frac{2}{\mathbf{v}^\top \mathbf{v}} = -\frac{1}{\sigma \mathbf{v}[1]}.$$

The transformed vector, $\mathbf{P}_{\mathbf{v}} \mathbf{x} = \sigma \hat{\mathbf{e}}_1$, has the same 2-norm as \mathbf{x} since $\mathbf{P}_{\mathbf{v}} = \mathbf{P}_{\mathbf{v}}^\top = \mathbf{P}_{\mathbf{v}}^{-1}$.

3.1.1. HQR: Algorithm. Given $\mathbf{A} \in \mathbb{R}^{m \times n}$ and Lemma 3.1, HQR is done by repeating the following processes until only an upper triangle matrix remains. For $i = 1, 2, \dots, n$,
 Step 1) Compute \mathbf{v} and β that zeros out the i^{th} column of \mathbf{A} beneath a_{ii} (see [alg. 2](#)), and
 Step 2) Apply $\mathbf{P}_{\mathbf{v}}$ to the bottom right partition, $\mathbf{A}[i : m, i : n]$ (lines 4-6 of [alg. 3](#)).

Consider the following 4-by-3 matrix example adapted from [\[15\]](#). Let \mathbf{P}_i represent the i^{th} HH transformation of this algorithm.

$$\mathbf{A} = \begin{bmatrix} \times & \times & \times \\ \times & \times & \times \\ \times & \times & \times \\ \times & \times & \times \end{bmatrix} \xrightarrow{\mathbf{P}_1 \mathbf{A}} \begin{bmatrix} \times & \times & \times \\ 0 & \times & \times \\ 0 & \times & \times \\ 0 & \times & \times \end{bmatrix} \xrightarrow{\mathbf{P}_2 \mathbf{P}_1 \mathbf{A}} \begin{bmatrix} \times & \times & \times \\ 0 & \times & \times \\ 0 & 0 & \times \\ 0 & 0 & \times \end{bmatrix} \xrightarrow{\mathbf{P}_3 \mathbf{P}_2 \mathbf{P}_1 \mathbf{A}} \begin{bmatrix} \times & \times & \times \\ 0 & \times & \times \\ 0 & 0 & \times \\ 0 & 0 & 0 \end{bmatrix}$$

The resulting matrix is the \mathbf{R} factor, $\mathbf{R} := \mathbf{P}_3 \mathbf{P}_2 \mathbf{P}_1 \mathbf{A}$, and the \mathbf{Q} factor for a full QR factorization is $\mathbf{Q} := \mathbf{P}_1 \mathbf{P}_2 \mathbf{P}_3$ since \mathbf{P}_i 's are symmetric. The thin factors for a general matrix $\mathbf{A} \in \mathbb{R}^{m \times n}$ are

$$(3.2) \quad \mathbf{Q}_{\text{thin}} = \mathbf{P}_1 \cdots \mathbf{P}_n \mathbf{I}_{m \times n} \quad \text{and} \quad \mathbf{R}_{\text{thin}} = \mathbf{I}_{m \times n}^\top \mathbf{P}_n \cdots \mathbf{P}_1 \mathbf{A}.$$

Algorithm 2: $\beta, \mathbf{v}, \sigma = \text{hhvec}(\mathbf{x})$. Given a vector $\mathbf{x} \in \mathbb{R}^m$, return $\mathbf{v} \in \mathbb{R}^m$ and $\beta, \sigma \in \mathbb{R}$ that satisfy $(\mathbf{I} - \beta \mathbf{v} \mathbf{v}^\top) \mathbf{x} = \sigma \hat{\mathbf{e}}_1$ and $\mathbf{v}[1] = 1$ (see [\[2, 15\]](#)).

Input: \mathbf{x}

Output: \mathbf{v}, σ , and β

```

1  $\mathbf{v} \leftarrow \text{copy}(\mathbf{x})$ 
2  $\sigma \leftarrow -\text{sign}(\mathbf{x}[1]) \|\mathbf{x}\|_2$ 
3  $\mathbf{v}[1] \leftarrow \mathbf{x}[1] - \sigma$ 
4  $\beta \leftarrow -\frac{\mathbf{v}[1]}{\sigma}$ 
5  $\mathbf{v} \leftarrow \mathbf{v} / \mathbf{v}[1]$ 
6 return  $\beta, \mathbf{v}, \sigma$ 
```

Algorithm 3: $\mathbf{V}, \beta, \mathbf{R} = \text{HQR2}(\mathbf{A})$. A Level-2 BLAS implementation of HQR. Given a matrix $\mathbf{A} \in \mathbb{R}^{m \times n}$ where $m \geq n$, return matrix $\mathbf{V} \in \mathbb{R}^{m \times n}$, vector $\beta \in \mathbb{R}^n$, and upper triangular matrix \mathbf{R} . The orthogonal factor \mathbf{Q} can be generated from \mathbf{V} and β .

Input: \mathbf{A}

Output: $\mathbf{V}, \beta, \mathbf{R}$

```

1 Initialize  $\mathbf{V} \leftarrow \mathbf{0}_{m \times n}$ ,  $\beta \leftarrow \mathbf{0}_m$ 
2 for  $i = 1 : n$  do
3    $\mathbf{v}, \beta, \sigma \leftarrow \text{hhvec}(\mathbf{A}[i : \text{end}, i])$  /* Algorithm 2 */
4    $\mathbf{V}[i : \text{end}, i], \beta_i, \mathbf{A}[i, i] \leftarrow \mathbf{v}, \beta, \sigma$ 
5    $\mathbf{A}[i + 1 : \text{end}, i] \leftarrow \text{zeros}(m - i)$ 
6    $\mathbf{A}[i : \text{end}, i + 1 : \text{end}] \leftarrow \mathbf{A}[i : \text{end}, i + 1 : \text{end}] - \beta \mathbf{v} \mathbf{v}^\top \mathbf{A}[i : \text{end}, i + 1 : \text{end}]$ 
7 return  $\mathbf{V}, \beta, \mathbf{A}[1 : n, 1 : n]$ 

```

3.1.2. HQR: Rounding Error Analysis. Now we present an error analysis for [alg. 3](#) by keeping track of the different operations of [alg. 2](#) and [alg. 3](#). We follow the analysis of [15] and modify it for the variant where $\mathbf{v}[1]$ is set to 1. The goal of this section is to present the basic steps of the standard error analysis for HQR so that we modify them easily in [section 4](#) for different mixed precision settings.

Calculating the i^{th} HH vector and constant. In [alg. 3](#), we compute the HH vector and constant by using [alg. 2](#) to $\mathbf{A}[i : m, i]$. For now, consider zeroing out any vector $\mathbf{x} \in \mathbb{R}^m$ below its first component with a HH transformation. We first calculate σ as is implemented in line 2 of [alg. 2](#).

$$(3.3) \quad \text{fl}(\sigma) = \hat{\sigma} = \text{fl}(-\text{sign}(\mathbf{x}[1])\|\mathbf{x}\|_2) = \sigma + \Delta\sigma, \quad |\Delta\sigma| \leq \gamma_{m+1}|\sigma|.$$

Note that the backward error incurred here accounts for an inner product of a vector in \mathbb{R}^m with itself and a square root operation to get the 2-norm. Let $\mathbf{v}'[1] \equiv \mathbf{x}[i] - \sigma$, the penultimate value $\mathbf{v}[1]$ held. The subtraction adds a single additional rounding error via

$$(3.4) \quad \text{fl}(\mathbf{v}'[1]) = \mathbf{v}'[1] + \Delta\mathbf{v}'[1] = (1 + \delta)(\mathbf{x}[i] - \sigma - \Delta\sigma) = (1 + \theta_{m+2})\mathbf{v}'[1]$$

where the last equality is granted because the sign of σ is chosen to prevent cancellation. Since [alg. 2](#) normalizes the HH vector so that its first component is 1, the remaining components of \mathbf{v} are divided by $\text{fl}(\tilde{\mathbf{v}}_1)$ incurring another single rounding error. As a result, the components of \mathbf{v} computed with FLOPs have error $\text{fl}(\mathbf{v}[j]) = \mathbf{v}[j] + \Delta\mathbf{v}[j]$ where

$$(3.5) \quad |\Delta\mathbf{v}[j]| \leq \gamma_{1+2(m+2)}|\mathbf{v}[j]| = \tilde{\gamma}_m|\mathbf{v}[j]| \quad j = 2 : m - i + 1,$$

and $|\Delta\mathbf{v}[1]| = 0$. Since $1 + 2(m + 2) = \mathcal{O}(m)$, we have swept that minor difference between under our use of the $\tilde{\gamma}$ notation defined in [Lemma 2.1](#). Next, we consider the HH constant, β , as is computed in line 4 of [alg. 2](#).

$$(3.6) \quad \hat{\beta} = \text{fl}(-\mathbf{v}'[1]/\hat{\sigma}) = -(1 + \delta) \frac{\mathbf{v}'[1] + \Delta\mathbf{v}'[1]}{\sigma + \Delta\sigma} = \frac{(1 + \delta)(1 + \theta_{m+2})}{(1 + \theta_{m+1})} \beta$$

$$(3.7) \quad = (1 + \theta_{3m+5})\beta = \beta + \Delta\beta, \quad \text{where } |\Delta\beta| \leq \tilde{\gamma}_m\beta.$$

We have shown (3.6) to keep our analysis simple in [section 4](#) and (3.7) show that the error incurred from calculating of $\|\mathbf{x}\|_2$ accounts for the vast majority of the rounding error so far. At iteration i , we replace \mathbf{x} with $\mathbf{A}[i : m, i] \in \mathbb{R}^{m-i+1}$ and the i^{th} HH constant and vector $(\hat{\beta}_i, \mathbf{v}_i)$ both have errors bounded by $\tilde{\gamma}_{m-i+1}$.

298 *Applying a Single HH Transformation.* Now we consider lines 4-6 of [alg. 3](#). At iteration i ,
 299 we set $\mathbf{A}[i+1 : m, :]$ to zero and replace $\mathbf{A}[i, i]$ with σ computed from [alg. 2](#). Therefore, we
 300 now need to calculate the errors for applying a HH transformation to the remaining columns,
 301 $\mathbf{A}[i : m, i+1 : n]$ with the computed HH vector and constant. This is the most crucial building
 302 block of the rounding error analysis for any variant of HQR because the \mathbf{R} factor is formed by
 303 applying the HH transformations to \mathbf{A} and the \mathbf{Q} factor is formed by applying them in reverse
 304 order to the identity. Both of the blocked versions in [subsection 3.2](#) and [subsection 3.3](#) also require
 305 slightly different but efficient implementations of this step. For example, BQR in [alg. 5](#) uses level-3
 306 BLAS operations to apply multiple HH transformations at once whereas the variant of HQR in
 307 [alg. 3](#) can only use level-2 BLAS operations to apply HH transformations.

308 A HH transformation is applied through a series of inner and outer products, since HH matrices
 309 are rank-1 updates of the identity. That is, computing $\mathbf{P}_{\mathbf{v}}\mathbf{x}$ for any $\mathbf{x} \in \mathbb{R}^m$ is as simple as computing

$$310 \quad (3.8) \quad \mathbf{y} := \mathbf{P}_{\mathbf{v}}\mathbf{x} = \mathbf{x} - (\beta\mathbf{v}^\top\mathbf{x})\mathbf{v}.$$

311 Let us assume that \mathbf{x} is an exact vector and there were errors incurred in forming \mathbf{v} and β . The
 312 errors incurred from computing \mathbf{v} and β need to be included in addition to the new rounding
 313 errors accumulating from the action of applying $\mathbf{P}_{\mathbf{v}}$ to a column. In practice, \mathbf{x} is any column in
 314 $\mathbf{A}^{(i-1)}[i+1 : m, i+1 : n]$, where the superscript $(i-1)$ indicates that this submatrix of \mathbf{A} has
 315 already been transformed by $i-1$ HH transformations that zeroed out components below $\mathbf{A}[j, j]$
 316 for $j = 1 : i-1$. We show the error for forming $\hat{\mathbf{w}}$ where $\mathbf{w} := \beta\mathbf{v}^\top\mathbf{x}\mathbf{v}$ and $\mathbf{v}, \mathbf{x} \in \mathbb{R}^m$,

$$317 \quad \hat{\mathbf{w}} = \text{fl}(\hat{\beta} \text{fl}(\hat{\mathbf{v}}^\top\mathbf{x})\hat{\mathbf{v}}) = (1 + \theta_m)(1 + \delta)(1 + \delta')(\beta + \Delta\beta)(\mathbf{v} + \Delta\mathbf{v})^\top\mathbf{x}(\mathbf{v} + \Delta\mathbf{v}),$$

318 where θ_m is from computing the inner product $\hat{\mathbf{v}}^\top\mathbf{x}$, and δ and δ' are from multiplying β , $\text{fl}(\hat{\mathbf{v}}^\top\mathbf{x})$,
 319 and $\hat{\mathbf{v}}$. The forward error is $\hat{\mathbf{w}} = \mathbf{w} + \Delta\mathbf{w}$, where $|\Delta\mathbf{w}| \leq \tilde{\gamma}_m|\beta||\mathbf{v}||\mathbf{v}|^\top|\mathbf{x}|$. Subtracting $\hat{\mathbf{w}}$ from \mathbf{x}
 320 yields the HH transformation with forward error,

$$321 \quad (3.9) \quad \text{fl}(\hat{\mathbf{P}}_{\mathbf{v}}\mathbf{x}) = \text{fl}(\mathbf{x} - \hat{\mathbf{w}}) = (1 + \delta)(\mathbf{x} - \mathbf{w} - \Delta\mathbf{w}) = \mathbf{y} + \Delta\mathbf{y} = (\mathbf{P}_{\mathbf{v}} + \Delta\mathbf{P}_{\mathbf{v}})\mathbf{x},$$

322 where $|\Delta\mathbf{y}| \leq u|\mathbf{x}| + \tilde{\gamma}_m|\beta||\mathbf{v}||\mathbf{v}|^\top|\mathbf{x}|$. Using $\sqrt{2/\beta} = \|\mathbf{v}\|_2$, we form a normwise bound,

$$323 \quad (3.10) \quad \|\Delta\mathbf{y}\|_2 \leq \tilde{\gamma}_m\|\mathbf{x}\|_2.$$

324 Since $\Delta\mathbf{P}_{\mathbf{v}}[i, j] = \frac{1}{\|\mathbf{x}\|_2^2}\Delta\mathbf{y}[i]\mathbf{x}[j]$, we can compute its Frobenius norm,

$$325 \quad (3.11) \quad \|\Delta\mathbf{P}_{\mathbf{v}}\|_F = \left(\sum_{i=1}^m \sum_{j=1}^m \left(\frac{1}{\|\mathbf{x}\|_2^2} \Delta\mathbf{y}[i]\mathbf{x}[j] \right)^2 \right)^{1/2} = \frac{\|\Delta\mathbf{y}\|_2}{\|\mathbf{x}\|_2} \leq \tilde{\gamma}_m,$$

326 where the last inequality is a direct application of [\(3.10\)](#).

327 *Applying many successive HH transformations.* Consider applying a sequence of transforma-
 328 tions in the set $\{\mathbf{P}_i\}_{i=1}^r \subset \mathbb{R}^{m \times m}$ to $\mathbf{x} \in \mathbb{R}^m$, where \mathbf{P}_i 's are all HH transformations computed with
 329 $\hat{\mathbf{v}}_i$'s and $\hat{\beta}_i$'s. This is directly applicable to HQR as $\mathbf{Q} = \mathbf{P}_1 \cdots \mathbf{P}_n \mathbf{I}$ and $\mathbf{R} = \mathbf{Q}^\top \mathbf{A} = \mathbf{P}_n \cdots \mathbf{P}_1 \mathbf{A}$.
 330 [Lemma 3.2](#) is very useful for any sequence of transformations, where each transformation has a
 331 known bound. We will invoke this lemma to prove [Lemma 3.3](#), and use it in future sections for
 332 other consecutive transformations.

LEMMA 3.2. If $\mathbf{X}_j + \Delta\mathbf{X}_j \in \mathbb{R}^{m \times m}$ satisfies $\|\Delta\mathbf{X}_j\|_F \leq \delta_j \|\mathbf{X}_j\|_2$ for all j , then

$$\left\| \prod_{j=1}^n (\mathbf{X}_j + \Delta\mathbf{X}_j) - \prod_{j=1}^n \mathbf{X}_j \right\|_F \leq \left(-1 + \prod_{j=1}^n (1 + \delta_j) \right) \prod_{j=1}^n \|\mathbf{X}_j\|_2.$$

LEMMA 3.3. Consider applying a sequence of transformations $\mathbf{Q} = \mathbf{P}_r \cdots \mathbf{P}_2 \mathbf{P}_1$ onto vector $\mathbf{x} \in \mathbb{R}^m$ to form $\hat{\mathbf{y}} = \mathbf{fl}(\hat{\mathbf{P}}_r \cdots \hat{\mathbf{P}}_2 \hat{\mathbf{P}}_1 \mathbf{x})$, where $\hat{\mathbf{P}}_k$'s are HH transformations constructed from $\hat{\beta}_k$ and $\hat{\mathbf{v}}_k$. These HH vectors and constants are computed via [alg. 2](#) and the rounding errors are bounded by (3.5) and (3.7). If each transformation is computed via (3.8), then

$$(3.12) \quad \hat{\mathbf{y}} = \mathbf{Q}(\mathbf{x} + \Delta\mathbf{x}) = (\mathbf{Q} + \Delta\mathbf{Q})\mathbf{x} = \hat{\mathbf{Q}}\mathbf{x},$$

$$(3.13) \quad \|\Delta\mathbf{y}\|_2 \leq r\tilde{\gamma}_m \|\mathbf{x}\|_2, \quad \|\Delta\mathbf{Q}\|_F \leq r\tilde{\gamma}_m.$$

Proof. Applying Lemma 3.2 directly to \mathbf{Q} yields

$$\|\Delta\mathbf{Q}\|_F = \left\| \prod_{j=1}^r (\mathbf{P}_j + \Delta\mathbf{P}_j) - \prod_{j=1}^r \mathbf{P}_j \right\|_F \leq \left(-1 + \prod_{j=1}^r (1 + \tilde{\gamma}_{m-j+1})^r \right) \prod_{j=1}^r \|\mathbf{P}_j\|_2 \leq -1 + (1 + \tilde{\gamma}_m)^r,$$

since \mathbf{P}_j 's are orthogonal and have 2-norm, 1, and $m - j + 1 \leq m$. While we omit the details here, we can show that $(1 + \tilde{\gamma}_m)^r - 1 \leq r\tilde{\gamma}_m$ using the argument from Lemma 2.1 if $r\tilde{\gamma}_m \leq 1/2$. \square

In this error analysis, the prevailing bound for errors at various stages of forming and applying a HH transformation is $\tilde{\gamma}_m$ where m corresponds to the dimension of the transformed vectors. In Lemma 3.3, a factor of r is introduced for applying r HH transformations to form the term $r\tilde{\gamma}_m \approx rmu$. Therefore, we can expect that the columnwise norm error for a thin QR factorization should be $\mathcal{O}(mnu)$ for a full rank matrix. In Theorem 3.4, we formalize this by applying Lemma 3.3 directly and also show a conversion of columnwise bounds to a matrix norm bound,

$$\|\Delta\mathbf{R}\|_F = \left(\sum_{i=1}^n \|\Delta\mathbf{R}[:, i]\|_2^2 \right)^{1/2} \leq \left(\sum_{i=1}^n n^2 \tilde{\gamma}_m^2 \|\mathbf{A}[:, i]\|_2^2 \right)^{1/2} = n\tilde{\gamma}_m \|\mathbf{A}\|_F.$$

We gather these results into Theorem 3.4.

THEOREM 3.4. Let $\mathbf{A} \in \mathbb{R}^{m \times n}$ with $m \geq n$ have full rank, n . Let $\hat{\mathbf{Q}} \in \mathbb{R}^{m \times n}$ and $\hat{\mathbf{R}} \in \mathbb{R}^{n \times n}$ be the thin QR factors of \mathbf{A} obtained via [alg. 3](#). Then,

$$\hat{\mathbf{R}} = \mathbf{R} + \Delta\mathbf{R} = \mathbf{fl}(\hat{\mathbf{P}}_n \cdots \hat{\mathbf{P}}_1 \mathbf{A}), \quad \|\Delta\mathbf{R}[:, j]\|_2 \leq n\tilde{\gamma}_m \|\mathbf{A}[:, j]\|_2, \quad \|\Delta\mathbf{R}\|_F \leq n\tilde{\gamma}_m \|\mathbf{A}\|_F$$

$$\hat{\mathbf{Q}} = \mathbf{Q} + \Delta\mathbf{Q} = \mathbf{fl}(\hat{\mathbf{P}}_1 \cdots \hat{\mathbf{P}}_n \mathbf{I}), \quad \|\Delta\mathbf{Q}[:, j]\|_2 \leq n\tilde{\gamma}_m, \quad \|\Delta\mathbf{Q}\|_F \leq n^{3/2} \tilde{\gamma}_m.$$

In future sections, we show the forward error columnwise bounds for each factor which can be easily converted to matrix norm bounds. The numerical experiments in [section 5](#) measure backward errors with $\|\hat{\mathbf{Q}}\hat{\mathbf{R}} - \mathbf{A}\|_F$ and the orthogonality of the \mathbf{Q} factor with $\|\hat{\mathbf{Q}}^T \hat{\mathbf{Q}} - \mathbf{I}\|_2$.

The content of this section shows the standard rounding error analysis in [15] where some important stages are summarized in (3.5), (3.7), and (3.13), which we will modify to different mixed precision settings in [section 4](#). These quantities account for various forward and backward errors formed in computing essential components of HQR, namely the HH constant and vector, as well as normwise errors of the action of applying HH transformations. In the next sections, we present blocked variants of HQR that use [alg. 3](#).

366 **3.2. Block HQR with partitioned columns (BQR).** We refer to the blocked variant
 367 of HQR where the columns are partitioned as BQR. Note that this section relies on the WY
 368 representation described in [5] instead of the storage-efficient version of [22], even though both are
 369 known to be just as numerically stable as HQR.

370 **3.2.1. The WY Representation.** A convenient matrix representation that accumulates r
 371 HH reflectors is known as the WY representation (see [5, 12]). Lemma 3.5 shows how to update
 372 a rank- j update of the identity, $\mathbf{Q}^{(j)}$, with a HH transformation, \mathbf{P} , to produce a rank- $(j+1)$
 373 update of the identity, $\mathbf{Q}^{(j+1)}$. With the correct initialization of \mathbf{W} and \mathbf{Y} , we can build the WY
 374 representation of successive HH transformations as shown in Algorithm 4. This algorithm assumes
 375 that the HH vectors, \mathbf{V} , and constants, β , have already been computed. Since the \mathbf{Y} factor is
 376 exactly \mathbf{V} , we only need to compute the \mathbf{W} factor.

377 LEMMA 3.5. Suppose $\mathbf{X}^{(j)} = \mathbf{I} - \mathbf{W}^{(j)}\mathbf{Y}^{(j)\top} \in \mathbb{R}^{m \times m}$ is an orthogonal matrix with $\mathbf{W}^{(j)}, \mathbf{Y}^{(j)} \in$
 378 $\mathbb{R}^{m \times j}$. Let us define $\mathbf{P} = \mathbf{I} - \beta \mathbf{v}\mathbf{v}^\top$ for some $\mathbf{v} \in \mathbb{R}^m$ and let $\mathbf{z}^{(j+1)} = \beta \mathbf{X}^{(j)}\mathbf{v}$. Then,

$$379 \quad \mathbf{X}^{(j+1)} = \mathbf{X}^{(j)}\mathbf{P} = \mathbf{I} - \mathbf{W}^{(j+1)}\mathbf{Y}^{(j+1)\top},$$

380 where $\mathbf{W}^{(j+1)} = [\mathbf{W}^{(j)} | \mathbf{z}]$ and $\mathbf{Y}^{(j+1)} = [\mathbf{Y}^{(j)} | \mathbf{v}]$ are each m -by- $(j+1)$.

Algorithm 4: $\mathbf{W}, \mathbf{Y} \leftarrow \text{buildWY}(V, \beta)$: Given a set of householder vectors $\{\mathbf{V}[:, i]\}_{i=1}^r$
 and their corresponding constants $\{\beta_i\}_{i=1}^r$, form the final \mathbf{W} and \mathbf{Y} factors of the WY
 representation of $\mathbf{P}_1 \cdots \mathbf{P}_r$, where $\mathbf{P}_i := \mathbf{I}_m - \beta_i \mathbf{v}_i \mathbf{v}_i^\top$

Input: $\mathbf{V} \in \mathbb{R}^{m \times r}$, $\beta \in \mathbb{R}^r$ where $m > r$.

Output: \mathbf{W}

```

1 Initialize:  $\mathbf{W} := \beta_1 \mathbf{V}[:, 1]$ . /*  $\mathbf{Y}$  is  $\mathbf{V}$ . */
2 for  $j = 2 : r$  do
3    $\mathbf{z} \leftarrow \beta_j [\mathbf{V}[:, j] - \mathbf{W}(\mathbf{V}[:, 1:j-1]^\top \mathbf{V}[:, j])]$ 
4    $\mathbf{W} \leftarrow [\mathbf{W} \quad \mathbf{z}]$  /* Update  $\mathbf{W}$  to an  $m$ -by- $j$  matrix. */
5 return  $\mathbf{W}$ 
```

381 In HQR, \mathbf{A} is transformed into an upper triangular matrix \mathbf{R} by identifying a HH transformation
 382 that zeros out a column below the diagonal, then applying that HH transformation to the bottom
 383 right partition. For example, the k^{th} HH transformation finds an $m-k+1$ sized HH transformation
 384 that zeros out column k below the diagonal and then applies it to the $(m-k+1)$ -by- $(n-k)$
 385 partition of the matrix, $\mathbf{A}[k : m, k+1 : n]$. Since the $k+1^{\text{st}}$ column is transformed by the
 386 k^{th} HH transformation, this algorithm must be executed serially as shown in alg. 3. The highest
 387 computational burden at each iteration falls on alg. 3 line 6, which requires Level-2 BLAS operations
 388 when computed efficiently.

389 In contrast, BQR replaces this step with Level-3 BLAS operations by partitioning \mathbf{A} into blocks
 390 of columns. Let $\mathbf{A} = [\mathbf{C}_1 \cdots \mathbf{C}_N]$ where $\mathbf{C}_1, \dots, \mathbf{C}_{N-1}$ are each m -by- r , and \mathbf{C}_N holds the remaining
 391 columns. The k^{th} block, \mathbf{C}_k , is transformed with HQR (alg. 3), and the WY representation of these
 392 r successive HH transformations is constructed as in alg. 4. We write the WY update as

$$393 \quad (3.14) \quad \mathbf{X}_k = \mathbf{I}_m - \mathbf{W}_k \mathbf{Y}_k^\top = \mathbf{P}_k^{(1)} \cdots \mathbf{P}_k^{(r)}.$$

Thus far, [algs. 3](#) and [4](#) are rich in Level-2 BLAS operations. Next, $\mathbf{I} - \mathbf{Y}_k \mathbf{W}_k^\top$ is applied to $[\mathbf{C}_2 \cdots \mathbf{C}_N]$ with two Level-3 BLAS operations as shown in line 5 of [alg. 5](#). BQR performs approximately $1 - \mathcal{O}(1/N)$ fraction of its FLOPs in Level-3 BLAS operations (see section 5.2.3 of [\[12\]](#)), and can reap the benefits from the accelerated block FMA feature of TensorCore. Note that BQR does require strictly more FLOPs when compared to HQR, but these additional FLOPs are negligible in standard precision and does not impact the numerical stability. A pseudoalgorithm for BQR is shown in [alg. 5](#) where we assume that $n = Nr$ to make our error analysis in [section 3.2.2](#) simple. In practice, an efficient implementation might require r to be a power of two or a product of small prime factors and result a thinner N^{th} block compared to the rest. This discrepancy is easily fixed by padding the matrix with zeros, a standard procedure for standard algorithms like the Fast Fourier Transform (FFT). For any variable x in $\{\mathbf{X}, \mathbf{W}, \mathbf{Y}, \mathbf{z}, \beta, \mathbf{v}, \mathbf{P}\}$, $x_k^{(j)}$ corresponds to the j^{th} update for the k^{th} block.

Algorithm 5: $\mathbf{Q}, \mathbf{R} \leftarrow \text{blockHQR}(\mathbf{A}, r)$: Perform HH QR factorization of matrix \mathbf{A} with column partitions of size r .

Input: $\mathbf{A} \in \mathbb{R}^{m \times n}$, $r \in \mathbb{R}$ where $r < n$.
Output: \mathbf{Q}, \mathbf{R}

```

1  $N = \frac{n}{r}$ 
  // Let  $\mathbf{A} = [\mathbf{C}_1 \cdots \mathbf{C}_N]$  where all blocks except  $\mathbf{C}_N$  are  $m$ -by- $r$  sized.
2 for  $i = 1 : N$  do
3    $\mathbf{V}_i, \beta_i, \mathbf{C}_i \leftarrow \text{hhQR}(\mathbf{C}_i)$                                      /* Algorithm 3 */
4    $\mathbf{W}_i \leftarrow \text{buildWY}(\mathbf{V}_i, \beta_i)$                                    /* Algorithm 4 */
5    $[\mathbf{C}_{i+1} \cdots \mathbf{C}_N] \leftarrow \mathbf{V}_i (\mathbf{W}_i^\top [\mathbf{C}_{i+1} \cdots \mathbf{C}_N])$  /* update the rest: BLAS-3 */
  //  $\mathbf{A}$  has been transformed into  $\mathbf{R} = \mathbf{Q}^\top \mathbf{A}$ .
  // Now build  $\mathbf{Q}$  using level-3 BLAS operations.
6  $\mathbf{Q} \leftarrow \mathbf{I}$                                                          /*  $\mathbf{I}_m$  if full QR, and  $\mathbf{I}_{m \times n}$  if thin QR. */
7 for  $i = N : -1 : 1$  do
8    $\mathbf{Q}[(i-1)r+1 : m, (i-1)r+1 : n] \leftarrow \mathbf{W}_i (\mathbf{V}_i^\top \mathbf{Q}[(i-1)r+1 : m, (i-1)r+1 : n])$ 
9 return  $\mathbf{Q}, \mathbf{A}$ 
```

3.2.2. BQR: Rounding Error Analysis. We now present the basic structure for the rounding error analysis for [alg. 5](#), which consist of: 1)HQR, 2)building the \mathbf{W} factor, and 3) updating the remaining blocks with the \mathbf{WY} representation. We have adapted the analysis from [\[15\]](#) to fit this exact variant, and denote $\hat{\mathbf{Q}}_{BQR}, \hat{\mathbf{R}}_{BQR}$ to be the outputs from [alg. 5](#). First, we analyze the error accumulated from updating $\mathbf{X}_k^{(j-1)}$ to $\mathbf{X}_k^{(j)}$, which applies a rank-1 update via the subtraction of the outer product $\hat{\mathbf{z}}_k^{(j)} \hat{\mathbf{v}}_k^{(j)\top}$. Since $\mathbf{z}_k^{(j)} = \beta_k^{(j)} \mathbf{X}_k^{(j-1)} \mathbf{v}_k^{(j)}$, this update requires a single HH transformation on the right side in the same efficient implementation that is discussed in [\(3.8\)](#),

$$(3.15) \quad \hat{\mathbf{X}}_k^{(j)} = \hat{\mathbf{X}}_k^{(j-1)} - \text{fl}(\hat{\beta}_k^{(j-1)} \hat{\mathbf{X}}_k^{(j-1)} \hat{\mathbf{v}}_k^{(j-1)}) \hat{\mathbf{v}}_k^{(j)\top} = \hat{\mathbf{X}}_k^{(j-1)} (\mathbf{P}_k^{(j)} + \Delta \mathbf{P}_k^{(j)}),$$

where $\|\Delta \mathbf{P}_k^{(j)}\|_F \leq \tilde{\gamma}_{m-(k-1)r}$. Since $\hat{\mathbf{X}}_k^{(1)} = \mathbf{I} - \hat{\beta}_k^{(1)} \hat{\mathbf{v}}_k^{(1)} \hat{\mathbf{v}}_k^{(1)\top} = \mathbf{P}_k^{(1)} + \Delta \mathbf{P}_k^{(1)}$, we can travel up the recursion relation in [\(3.15\)](#) and use [Lemma 3.2](#) to form

$$(3.16) \quad \|\Delta \mathbf{X}_k^{(j)}\|_F \leq j \tilde{\gamma}_{m-(k-1)r}.$$

417 *HQR within each block: line 3 of alg. 5.* We apply Algorithm 3 to the k^{th} block, $\hat{\mathbf{X}}_{k-1} \cdots \hat{\mathbf{X}}_1 \mathbf{C}_k$,
 418 which applies r more HH transformations to columns that had been transformed by $(k-1)$ WY
 419 transformations in prior iterations. The upper trapezoidal factor that results from applying HQR
 420 to $\mathbf{C}_k^{((k-1)r)}$ corresponds to the $(k-1)r+1^{st}$ to kr^{th} columns of $\hat{\mathbf{R}}_{BQR}$, and applying Lemmas 3.2
 421 and 3.3 yields

$$422 \quad \|\hat{\mathbf{R}}_{BQR}[:, j] - \mathbf{R}[:, j]\|_2 \leq r\tilde{\gamma}_m \|\hat{\mathbf{X}}_{k-1} \cdots \hat{\mathbf{X}}_1^\top \mathbf{C}_k[:, j]\|_2, \quad j = (k-1)r+1 : kr.$$

423 *Build WY at each block: line 4 of alg. 5.* We now calculate the rounding errors incurred from
 424 building the WY representation when given a set of HH vectors and constants as shown in alg. 4.
 425 Since the columns of $\hat{\mathbf{Y}}_k$ are simply $\{\hat{\mathbf{v}}_k^{(j)}\}$ built in alg. 3 the errors for forming these are shown in
 426 (3.5) where m should be replaced by $m - (k-1)r$. The HH constants, $\hat{\beta}_k^{(j)}$ are bounded by (3.7)
 427 modified similarly. Thus, $\mathbf{z}_k^{(j)}$ is the only newly computed quantity. Using (3.5), (3.7), and (3.16),
 428 we find

$$429 \quad \|\Delta \mathbf{z}_k^{(j)}\|_2 = \|\Delta \mathbf{X}_k^{(j-1)} \hat{\beta}_k^{(j)} \hat{\mathbf{v}}_k^{(j)}\|_2 \leq \|\Delta \mathbf{X}_k^{(j-1)}\|_2 \|\hat{\beta}_k^{(j)} \hat{\mathbf{v}}_k^{(j)}\|_2 \leq \|\Delta \mathbf{X}_k^{(j-1)}\|_F \|\hat{\beta}_k^{(j)} \hat{\mathbf{v}}_k^{(j)}\|_2 \\ 430 \quad \leq ((1 + (j-1)\tilde{\gamma}_{m-(k-1)r})(1 + \tilde{\gamma}_{m-(k-1)r}) - 1) \|\beta_k^{(j)} \mathbf{v}_k^{(j)}\|_2 \leq j\tilde{\gamma}_{m-(k-1)r} \|\mathbf{z}_k^{(j)}\|_2.$$

432 Componentwise bounds follow immediately, and are summarized in Lemma 3.6.

433 **LEMMA 3.6.** *Consider the construction of the WY representation for the k^{th} partition of matrix*
 434 $\mathbf{A} \in \mathbb{R}^{m \times n}$ *given a set of HH constants and vectors, $\{\beta_k^{(j)}\}_{j=1}^r$ and $\{\mathbf{v}_k^{(j)}\}$ via alg. 4. Then,*

$$435 \quad (3.17) \quad \hat{\mathbf{z}}_k^{(j)} = \mathbf{z}_k^{(j)} + \Delta \mathbf{z}_k^{(j)}, \quad |\Delta \mathbf{z}_k^{(j)}| \leq j\tilde{\gamma}_{m-(k-1)r} |\mathbf{z}_k^{(j)}|, \quad \|\Delta \mathbf{z}_k^{(j)}\|_2 \leq j\tilde{\gamma}_{m-(k-1)r} \|\mathbf{z}_k^{(j)}\|_2.$$

436 Most importantly, this shows that constructing the WY update is just as numerically stable as
 437 applying successive HH transformations (see Section 19.5 of [15]).

438 *Update blocks to the right: line 5 of alg. 5.* We now consider applying $\mathbf{X}_k := \mathbf{I} - \mathbf{W}_k \mathbf{Y}_k^\top$ to
 439 some matrix, \mathbf{B} . In practice, \mathbf{B} is the bottom right submatrix, $[\mathbf{C}_{k+1} \cdots \mathbf{C}_N][(k-1)r+1 : m, :]$.
 440 We can apply (3.16) directly to the columns of \mathbf{B} ,

$$441 \quad (3.18) \quad \|\mathbf{f}(\hat{\mathbf{X}}_k \mathbf{B}[:, j])\|_2 = \|\mathbf{f}(\hat{\mathbf{X}}_k^{(r)} \mathbf{B}[:, j])\|_2 \leq r\tilde{\gamma}_{m-(k-1)r} \|\mathbf{B}[:, j]\|_2$$

443 A normwise bound for employing a general matrix-matrix multiplication operation is stated in
 444 section 19.5 of [15].

445 *Multiple WY updates: line 8-9 of alg. 5.* All that remains is to consider the application of
 446 successive WY updates to form the QR factorization computed with BQR denoted as \mathbf{Q}_{BQR} and
 447 \mathbf{R}_{BQR} . We can apply Lemma 3.2 directly by setting $\mathbf{X}_k := \mathbf{I} - \mathbf{W}_k \mathbf{Y}_k^\top$ and consider the backward
 448 errors for applying the sequence to a vector, $\mathbf{x} \in \mathbb{R}^m$, as we did for Lemma 3.3. Since $\mathbf{X}_k =$
 449 $\mathbf{P}_{(k-1)r+1} \cdots \mathbf{P}_{kr}$, is simply a sequence of HH transformations, it is orthogonal, i.e. $\|\mathbf{X}_k\|_2 = 1$. We
 450 only need to replace with \mathbf{x} with $\mathbf{A}[:, i]$'s to form the columnwise bounds for \mathbf{R}_{BQR} , and apply the
 451 transpose to $\hat{\mathbf{e}}_i$'s to form the bounds for \mathbf{Q}_{BQR} . Then,

$$452 \quad (3.19) \quad \left\| \prod_{k=1}^N (\mathbf{X}_k + \Delta \mathbf{X}_k) - \prod_{k=1}^N \mathbf{X}_k \right\|_F \leq \left(-1 + \sum_{k=1}^N (1 + r\tilde{\gamma}_{m-(k-1)r}) \right) \leq rN\tilde{\gamma}_m \equiv n\tilde{\gamma}_m,$$

$$453 \quad (3.20) \quad \|\hat{\mathbf{Q}}_{BQR} - \mathbf{Q}\|_F \leq n^{3/2} \tilde{\gamma}_m.$$

We can also form the normwise bound for the j'^{th} column of $\hat{\mathbf{Q}}_{BQR}, \hat{\mathbf{R}}_{BQR}$. If we let $k' = \lceil j'/r \rceil^{th}$, then the j'^{th} column is the result of applying $k' - 1$ WY updates and an additional HQR. Applying Lemma 3.2 yields

$$(3.21) \quad \|\Delta \mathbf{R}_{BQR}[:, j']\|_2 \leq rk' \tilde{\gamma}_m \|\mathbf{A}[:, j']\|_2, \quad \|\Delta \mathbf{R}_{BQR}\|_F \leq n \tilde{\gamma}_m \|\mathbf{A}\|_F$$

$$(3.22) \quad \|\Delta \mathbf{Q}_{BQR}[:, j']\|_2 \leq rk' \tilde{\gamma}_m, \quad \|\Delta \mathbf{Q}_{BQR}\|_F = r \tilde{\gamma}_m \sum_{j=1}^n \lceil j/r \rceil = n^{3/2} \tilde{\gamma}_m.$$

and near orthogonality of the \mathbf{Q} factor is still achieved.

BQR and HQR error bound comparison. BQR under exact arithmetic is equivalent to HQR, and it is often referred to as the level-3 BLAS version of HQR. Furthermore, the error analysis of this section shows that BQR is as numerically stable as HQR despite requiring more FLOPs. In fact, many linear algebra libraries such as LAPACK use a variant of BQR as the QR factorization algorithm (see `dgeqrf` of [2]).

The primary goal of the analysis presented in this section is to provide the basic skeleton for the standard BQR rounding error analysis to make the generalization to mixed precision settings in section 4 easier. Readers should refer to [12, 15] for full details.

3.3. Block HQR with partitioned rows : Tall-and-Skinny QR (TSQR). Some important problems that require QR factorizations of overdetermined systems include least squares problems, eigenvalue problems, low rank approximations, as well as other matrix decompositions. Although Tall-and-Skinny QR (TSQR) broadly refers to block QR factorization methods with row partitions, we will discuss a specific variant of TSQR which is also known as the AllReduce algorithm [21]. In this paper, the TSQR/AllReduce algorithm refers to the most parallel variant of the block QR factorization algorithms discussed in [10]. A detailed description and rounding error analysis of this algorithm can be found in [21], and we present a pseudocode for the algorithm in alg. 6. Our initial interest in this algorithm came from its parallelizable nature, which is particularly suitable to implementation on GPUs. Additionally, our numerical simulations (discussed in section 5) show that TSQR can not only increase the speed but also outperform the traditional HQR factorization in low precisions.

3.3.1. TSQR/AllReduce Algorithm. Algorithm 6 partitions the rows of a tall-and-skinny matrix, \mathbf{A} . HQR is performed on each of those blocks and pairs of \mathbf{R} factors are combined to form the next set of \mathbf{A} matrices to be QR factorized. This process is repeated until only a single \mathbf{R} factor remains, and the \mathbf{Q} factor is built from all of the HH constants and vectors stored at each level. The most gains from parallelization can be made in the initial level where the maximum number of independent HQR factorizations occur. Although more than one configuration of this algorithm may be available for a given tall-and-skinny matrix, the number of nodes available and the shape of the matrix eliminate some of those choices. For example, a 1600-by-100 matrix can be partitioned into 2, 4, 8, or 16 initial row-blocks but may be restricted by a machine with only 4 nodes, and a 1600-by-700 matrix can only be partitioned into 2 initial blocks. Our numerical experiments show that the choice in the initial partition, which directly relates to the recursion depth of TSQR, has an impact in the accuracy of the QR factorization.

We refer to *level* as the number of recursions in a particular TSQR implementation. An L -level TSQR algorithm partitions the original matrix into $2^{(L)}$ submatrices in the initial or 0^{th} level of the algorithm, and 2^{L-i} QR factorizations are performed in level i for $i = 1, \dots, L$. The set of matrices that are QR factorized at each level i are called $\mathbf{A}_j^{(i)}$ for $j = 1, \dots, 2^{L-i}$, where superscript (i)

498 corresponds to the level and the subscript j indexes the row-blocks within level i . In the following
 499 sections, [alg. 6](#) (`tsqr`) will find a TSQR factorization of a matrix $A \in \mathbb{R}^{m \times n}$ where $m \gg n$. The
 500 inline function `qr` refers to [alg. 3](#) and we use [alg. 2](#) as a subroutine of `qr`.
 501 *TSQR Notation.* We introduce new notation due to the multi-level nature of the TSQR algo-
 502 rithm. In the final task of constructing \mathbf{Q} , $\mathbf{Q}_j^{(i)}$ factors are aggregated from each block at each level.
 503 Each $\mathbf{Q}_j^{(i)}$ factor from level i is partitioned such that two corresponding $\mathbf{Q}^{(i-1)}$ factors from level $i-1$
 504 can be applied to them. The partition (approximately) splits $\mathbf{Q}_j^{(i)}$ into two halves, $[\tilde{\mathbf{Q}}_{j,1}^{(i)\top} \tilde{\mathbf{Q}}_{j,2}^{(i)\top}]^\top$.
 505 The functions $\alpha(j)$ and $\phi(j)$ are defined such that $\mathbf{Q}_j^{(i)}$ is applied to the correct blocks from the level
 506 below: $\tilde{\mathbf{Q}}_{\alpha(j),\phi(j)}^{(i+1)}$. For $j = 1, \dots, 2^{L-i}$ at level i , we need $j = 2(\alpha(j) - 1) + \phi(j)$, where $\alpha(j) = \lceil \frac{j}{2} \rceil$
 507 and $\phi(j) = 2 + j - 2\alpha(j) \in \{1, 2\}$. [section 3.3.2](#) shows full linear algebra details for a single-level
 508 ($L = 1, 2$ initial blocks) example. The reconstruction of \mathbf{Q} can be implemented more efficiently (see

509 [4]), but the reconstruction method in [alg. 6](#) is presented for a clear, straightforward explanation.

Algorithm 6: $\mathbf{Q}, \mathbf{R} = \text{tsqr}(\mathbf{A}, L)$. Finds a QR factorization of a tall, skinny matrix, \mathbf{A} .

Input: $\mathbf{A} \in \mathbb{R}^{m \times n}$ where $m \gg n$, $L \leq \lfloor \log_2(\frac{m}{n}) \rfloor$, and 2^L is the initial number of blocks.

Output: $\mathbf{Q} \in \mathbb{R}^{m \times n}$, $\mathbf{R} \in \mathbb{R}^{n \times n}$ such that $\mathbf{QR} = \mathbf{A}$.

```

1  $h \leftarrow m2^{-L}$  // Number of rows.
/* Split  $\mathbf{A}$  into  $2^L$  blocks. Note that level  $(i)$  has  $2^{L-i}$  blocks. */
2 for  $j = 1 : 2^L$  do
3    $\mathbf{A}_j^{(0)} \leftarrow \mathbf{A}[(j-1)h + 1 : jh, :]$ 

   /* Store HH vectors as columns of matrix  $\mathbf{V}_j^{(i)}$ , HH constants as components of
      vector  $\beta_j^{(i)}$ , and set up the next level. */
4 for  $i = 0 : L - 1$  do
   /* The inner loop can be parallelized. */
5   for  $j = 1 : 2^{L-i}$  do
6      $\mathbf{V}_{2j-1}^{(i)}, \beta_{2j-1}^{(i)}, \mathbf{R}_{2j-1}^{(i)} \leftarrow \text{qr}(\mathbf{A}_{2j-1}^{(i)})$ 
7      $\mathbf{V}_{2j}^{(i)}, \beta_{2j}^{(i)}, \mathbf{R}_{2j}^{(i)} \leftarrow \text{qr}(\mathbf{A}_{2j}^{(i)})$ 
8      $\mathbf{A}_j^{(i+1)} \leftarrow \begin{bmatrix} \mathbf{R}_{2j-1}^{(i)} \\ \mathbf{R}_{2j}^{(i)} \end{bmatrix}$ 

9    $\mathbf{V}_1^{(L)}, \beta_1^{(L)}, \mathbf{R} \leftarrow \text{qr}(\mathbf{A}_1^{(L)})$  // The final  $\mathbf{R}$  factor is built.
10   $\mathbf{Q}_1^{(L)} \leftarrow \text{hh\_mult}(\mathbf{V}_1^{(L)}, I_{2n \times n})$ 
   /* Compute  $\mathbf{Q}^{(i)}$  factors by applying  $\mathbf{V}^{(i)}$  to  $\mathbf{Q}^{(i+1)}$  factors. */
11 for  $i = L - 1 : -1 : 1$  do
12   for  $j = 1 : 2^{L-i}$  do
13      $\mathbf{Q}_j^{(i)} \leftarrow \text{hh\_mult}\left(\mathbf{V}_j^{(i)}, \begin{bmatrix} \tilde{\mathbf{Q}}_{\alpha(j), \phi(j)}^{(i+1)} \\ \mathbf{0} \end{bmatrix}\right)$ 

14  $\mathbf{Q} \leftarrow []$ ; // Construct the final  $\mathbf{Q}$  factor.
15 for  $j = 1 : 2^L$  do
16    $\mathbf{Q} \leftarrow \begin{bmatrix} \mathbf{Q} \\ \text{hh\_mult}\left(\mathbf{V}_j^{(0)}, \begin{bmatrix} \tilde{\mathbf{Q}}_{\alpha(j), \phi(j)}^{(1)} \\ \mathbf{0} \end{bmatrix}\right) \end{bmatrix}$ 
17 return  $\mathbf{Q}, \mathbf{R}$ 

```

511 **3.3.2. Single-level Example.** In the single-level version of this algorithm, we first bisect \mathbf{A}
512 into $\mathbf{A}_1^{(0)}$ and $\mathbf{A}_2^{(0)}$ and compute the QR factorization of each of those submatrices. We combine the
513 resulting upper-triangular matrices (see below) which is QR factorized, and the process is repeated:

$$514 \quad \mathbf{A} = \begin{bmatrix} \mathbf{A}_1^{(0)} \\ \mathbf{A}_2^{(0)} \end{bmatrix} = \begin{bmatrix} \mathbf{Q}_1^{(0)} \mathbf{R}_1^{(0)} \\ \mathbf{Q}_2^{(0)} \mathbf{R}_2^{(0)} \end{bmatrix} = \begin{bmatrix} \mathbf{Q}_1^{(0)} & \mathbf{0} \\ \mathbf{0} & \mathbf{Q}_2^{(0)} \end{bmatrix} \begin{bmatrix} \mathbf{R}_1^{(0)} \\ \mathbf{R}_2^{(0)} \end{bmatrix} = \begin{bmatrix} \mathbf{Q}_1^{(0)} & \mathbf{0} \\ \mathbf{0} & \mathbf{Q}_2^{(0)} \end{bmatrix} \mathbf{A}_1^{(1)} = \begin{bmatrix} \mathbf{Q}_1^{(0)} & \mathbf{0} \\ \mathbf{0} & \mathbf{Q}_2^{(0)} \end{bmatrix} \mathbf{Q}_1^{(1)} \mathbf{R}.$$

515 The \mathbf{R} factor of $\mathbf{A}_1^{(1)}$ is the final \mathbf{R} factor of the QR factorization of the original matrix, \mathbf{A} . However,
516 the final \mathbf{Q} still needs to be constructed. Bisecting $\mathbf{Q}_1^{(1)}$ into two submatrices, i.e. $\tilde{\mathbf{Q}}_{1,1}^{(1)}$ and $\tilde{\mathbf{Q}}_{1,2}^{(1)}$,

allows us to write and compute the product more compactly,

$$\mathbf{Q} := \begin{bmatrix} \mathbf{Q}_1^{(0)} & \mathbf{0} \\ \mathbf{0} & \mathbf{Q}_2^{(0)} \end{bmatrix} \mathbf{Q}_1^{(1)} = \begin{bmatrix} \mathbf{Q}_1^{(0)} & \mathbf{0} \\ \mathbf{0} & \mathbf{Q}_2^{(0)} \end{bmatrix} \begin{bmatrix} \tilde{\mathbf{Q}}_{1,1}^{(1)} \\ \tilde{\mathbf{Q}}_{1,2}^{(1)} \end{bmatrix} = \begin{bmatrix} \mathbf{Q}_1^{(0)} \tilde{\mathbf{Q}}_{1,1}^{(1)} \\ \mathbf{Q}_2^{(0)} \tilde{\mathbf{Q}}_{1,2}^{(1)} \end{bmatrix}.$$

More generally, [alg. 6](#) takes a tall-and-skinny matrix \mathbf{A} and level L and finds a QR factorization by initially partitioning \mathbf{A} into $2^{(l)}$ row-blocks and includes the building of \mathbf{Q} . For simplicity, we assume that m is exactly $h2^{(l)}$ so that the initial partition yields $2^{(l)}$ blocks of equal sizes, h -by- n . Also, note that `hh_mult` refers to the action of applying multiple HH transformations given a set of HH vectors and constants, which can be performed by iterating line 6 of [alg. 3](#). This step can be done in a level-3 BLAS operation via a WY update if [alg. 6](#) was modified to store the WY representation at the QR factorization of each block of each level, $\mathbf{A}_j^{(i)}$.

3.3.3. TSQR: Rounding Error Analysis. The TSQR algorithm presented in [alg. 6](#) is a divide-and-conquer strategy for the QR factorization that uses the HQR within the subproblems. Divide-and-conquer methods can naturally be implemented in parallel and accumulate less rounding errors. For example, the single-level TSQR decomposition of a tall-and-skinny matrix, \mathbf{A} requires 3 total HQRs of matrices of sizes $\lfloor \log_2(\frac{m}{n}) \rfloor$ -by- n , $\lfloor \log_2(\frac{m}{n}) \rfloor$ -by- n , and $2n$ -by- n . The single-level TSQR strictly uses more FLOPs, but the dot product subroutines may accumulate smaller rounding errors (and certainly have smaller upper bounds) since they are performed on shorter vectors, and lead to a more accurate solution overall. These concepts are elucidated in [21] and we summarize the main results in [Theorem 3.7](#).

THEOREM 3.7. *Let $\mathbf{A} \in \mathbb{R}^{m \times n}$ with $m \geq n$ have full rank, n , and $\hat{\mathbf{Q}}_{TSQR} \in \mathbb{R}^{m \times n}$ and $\hat{\mathbf{R}}_{TSQR} \in \mathbb{R}^{n \times n}$ be the thin QR factors of \mathbf{A} obtained via [alg. 6](#) with L levels. Let us further assume that m is divisible by 2^L and $n\tilde{\gamma}_{m2^{-L}}, n\tilde{\gamma}_{2n} \ll 1$. Then, 2-norm error bound for the j^{th} column ($j = 1 : n$) of $\hat{\mathbf{R}}_{TSQR}$ and the Frobenius norm error bound for $\hat{\mathbf{Q}}_{TSQR}$ are*

$$(3.23) \quad \|\hat{\mathbf{R}}_{TSQR}[:, j] - \mathbf{R}[:, j]\|_2 \leq n(\tilde{\gamma}_{m2^{-L}} + L\tilde{\gamma}_{2n})\|\mathbf{A}[:, j]\|_2,$$

$$(3.24) \quad \|\hat{\mathbf{Q}}_{TSQR} - \mathbf{Q}\|_F \leq n^{3/2}(\tilde{\gamma}_{m2^{-L}} + L\tilde{\gamma}_{2n}).$$

Note that the $n\tilde{\gamma}_{m2^{-L}}$ and $n\tilde{\gamma}_{2n}$ terms correspond to errors from applying HQR to the blocks in the initial partition and to the blocks in levels 1 through L respectively. We can easily replace these with analogous mixed precision terms and keep the analysis accurate. Both level-2 and level-3 BLAS implementations will be considered in [section 4](#).

TSQR and HQR error bound comparison. We compare the error bounds for HQR and TSQR. Consider the bounds for $\|\hat{\mathbf{Q}} - \mathbf{Q}\|_F$ in [Theorems 3.4](#) and [3.7](#). TSQR has a lower worst-case error bound than HQR when integers $m, n > 0$, and $L \geq 0$ satisfy

$$1 \gg n^{3/2}\gamma^{(m)} \gg n^{3/2}(\gamma^{(\frac{m}{2^L})} + L\gamma^{(2n)}).$$

Let us consider as an example the case when $\frac{m}{2^L} = 2n$. Then, the HQR bound is $2^L/(L+1)$ larger than the bound for TSQR with L levels. For example, in single precision, a HQR of a 2^{15} -by- 2^6 matrix results in an upper bound relative backward error ($\|\mathbf{A} - \hat{\mathbf{Q}}\hat{\mathbf{R}}\|_F/\|\mathbf{A}\|_F$) of ≈ 1.002 , but a TSQR with $L = 8$ is bounded by $\approx 3.516\text{e-}02$. This case exemplifies a situation in which stability is not guaranteed in HQR, but the method is stable when using TSQR, even in the worst-case. Now consider some 2^{20} -by- 2^{12} matrix and QR factorizations performed with double precision. The error bound for HQR is $1.686\text{e-}7$, whereas the error bound for TSQR with 12 levels is $5.351\text{e-}10$.

In general, we can conjecture that values of L that can make $m2^{-L}$ and $2Ln$ much smaller than m , should produce a TSQR that outperforms HQR in worst-case scenarios, at least in uniform precision settings. However, the range of matrix sizes that TSQR can accommodate decreases as L grows larger. Figure 1 shows the matrix sizes HQR, 2-level TSQR, and 4-level TSQR can accommodate as well as their respective error bounds.

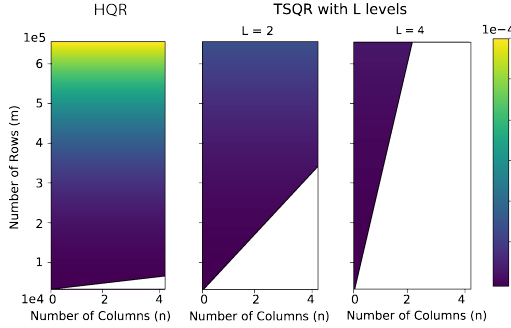


FIG. 1. Non-white space indicates allowable matrix sizes for each scheme, and color map represents error bounds for $\|\Delta\mathbf{Q}\|_F$ for uniform precision error analysis when using double precision arithmetic.

ponentwise forward error is,

$$\text{castdown}_l(\mathbf{x}) = \mathbf{x} + \Delta\mathbf{x}, \quad |\Delta\mathbf{x}| < u^{(l)}|\mathbf{x}|.$$

We use this to represent the backward error of a casting down a vector with a linear transformation, $\mathbf{I}^{(l)} := \mathbf{I} + \mathbf{E} \in \mathbb{R}^{m \times m}$, a diagonal perturbation of the identity. We write,

$$(4.1) \quad \mathbf{x}^{(l)} := \text{castdown}(\mathbf{x}^{(h)}) = \mathbf{I}^{(l)}\mathbf{x}^{(h)} = (\mathbf{I} + \mathbf{E})\mathbf{x}^{(h)} = \mathbf{x}^{(h)} + \Delta\mathbf{x},$$

where $|\Delta\mathbf{x}| \leq u^{(l)}|\mathbf{x}^{(h)}|$ and $\|\Delta\mathbf{x}\|_2 \leq u^{(l)}\|\mathbf{x}^{(h)}\|_2$. Thus, $\mathbf{E} = \Delta\mathbf{x}\mathbf{x}^\top / \|\mathbf{x}\|_2^2$ and we can use the same argument as in (3.11) to form a backward matrix norm bound,

$$(4.2) \quad \|\mathbf{E}\|_F \leq u^{(l)}.$$

Casting down after HQR in high precision. Let us consider the trivial case of carrying out HQR in high precision and casting down at the very end. This is useful for the analysis of mixed precision block algorithms as will be shown in subsection 4.1. If the two floating point types \mathbb{F}_l and \mathbb{F}_h satisfy $\mathbb{F}_l \subseteq \mathbb{F}_h$ and the matrix to be factorized is stored with low precision numbers, $\mathbf{A} \in \mathbb{F}_l^{m \times n}$, then casting up adds no rounding errors. Therefore, we can directly apply the analysis that culminated in Theorem 3.4, and we only consider the columnwise forward error in the \mathbf{Q} factor. Then, the j^{th} column of $\hat{\mathbf{Q}}_{HQR} = \mathbf{Q} + \Delta\mathbf{Q}_{HQR}$ is bounded normwise via $\|\Delta\mathbf{Q}_{HQR}[:, j]\|_2 \leq n\tilde{\gamma}_m^h$, and incurs an extra rounding error when $\hat{\mathbf{Q}}_{HQR} \in \mathbb{F}_h^{m \times n}$ is cast down to $\mathbb{F}_l^{m \times n}$. Using this in Lemma 3.2 to analyze the forward norm error for the j^{th} column of the \mathbf{Q} factor computed with alg. 3 yields

$$(4.3) \quad \|(\text{castdown}(\hat{\mathbf{Q}}_{HQR}) - \mathbf{Q})[:, j]\|_2 = \|(\mathbf{I}^{(l)}\hat{\mathbf{P}}_1 \cdots \hat{\mathbf{P}}_n - \mathbf{P}_1 \cdots \mathbf{P}_n)\hat{\mathbf{e}}_j\|_2 \leq u^{(l)} + n\tilde{\gamma}_m^{(h)} + nu^{(l)}\tilde{\gamma}_m^{(h)}.$$

4. Mixed precision error analysis.

In this section, we consider three different mixed precision settings for the QR factorization, all of which take in a matrix \mathbf{A} stored in low precision and return \mathbf{Q}, \mathbf{R} both represented in low precision. First, we consider a trivial mixed precision setting where HQR, BQR, and TSQR are computed in high precision after casting up the input matrix at the beginning, and casting down the resulting high precision factors to low precision. Then in subsection 4.1, we modify BQR and TSQR to utilize level-3 BLAS operations and TensorCore bFMAs for the matrix product subroutines. Finally, we impose MP Setting 2.3 in subsection 4.2 to see how a mixed precision inner product impacts HQR, BQR, and TSQR when applied in level-2 BLAS operations.

Backward error of casting down vectors. First, consider casting down a vector $\mathbf{x} \in \mathbb{F}_h^{(m)}$. The com-

598 The final castdown operation increases the upper bound by $u^{(l)}$ and the size of \mathbf{A} has no impact on
 599 this extra rounding error. Applying this trivial mixed precision setting to BQR and TSQR would
 600 simply increase the error bound by approximately $u^{(l)}$ all the while taking an even longer time
 601 than the high precision implementation due the extra cast down and cast up operations. Therefore,
 602 we do not analyze the rounding error analysis of this mixed precision variant of BQR and TSQR.
 603 However, we will use this mixed precision HQR as a subroutine of the mixed precision BQR and
 604 TSQR in the following section.

605 **4.1. Round down at block-level: level-3 BLAS mixed precision setting.** The mixed
 606 precision setting in this section is designed to meet the below requirements.

- 607 1. Modify Algorithms 5 and 6 to maximize level-3 BLAS operations and use TensorCore
 608 bFMAs.
- 609 2. Apply (4.3) to all instances of HQR to the error analyses for BQR and TSQR in section 3.
- 610 3. Cast down quantities at every block/level and the insertion of low precision errors $u^{(l)}$
 611 should be somewhat correlated to the number of blocks and levels.
- 612 4. Both input and output of the various QR factorization algorithms are given in the low
 613 precision.

614 TensorCore's bFMA computes

$$615 \quad (4.4) \quad \hat{\mathbf{D}} = \text{fl}_{TC}(\mathbf{C} + \mathbf{A}\mathbf{B}), \quad \mathbf{C}, \mathbf{D} \in \mathbb{F}_{\text{fp16}}^{4 \times 4} \text{ or } \mathbb{F}_{\text{fp32}}^{4 \times 4}, \text{ and } \mathbf{A}, \mathbf{B} \in \mathbb{F}_{\text{fp16}}^{4 \times 4},$$

616 and employs *full* precision products and fp32 summation accumulate. Here, the *full* precision
 617 multiplication is exact as explained in section 2. In [6], the authors investigate all four possible
 618 matrix-matrix multiplication routines in TensorCore, which depend on whether \mathbf{C} and \mathbf{D} are com-
 619 puted in fp16 or fp32. They also note that matrices larger than 4-by-4 can still be computed using
 620 this block FMA by accumulating matrix sums with $\mathbf{C} \in \mathbb{F}_{\text{fp32}}^{4 \times 4}$. Suppose that we aim to compute
 621 a fp16 matrix product of two fp16 matrices, $\mathbf{X} \in \mathbb{F}_{(fp16)}^{m \times p}$, $\mathbf{Y} \in \mathbb{F}_{(fp16)}^{p \times n}$, and $\mathbf{Z} = \mathbf{X}\mathbf{Y} \in \mathbb{F}_{\text{fp16}}^{m \times n}$. We
 622 pad \mathbf{X}, \mathbf{Y} with zeros so that all matrix dimensions are multiples of 4 and the matrix product can
 623 be computed with the TensorCore block FMA. Let $\mathbf{Q}_{[i,j]} := \mathbf{Q}[4(i-1)+1 : 4i, 4(j-1)+1 : 4j]$
 624 refer to the $(i, j)^{th}$ 4-by-4 block for any $\mathbf{Q} \in \{\mathbf{X}, \mathbf{Y}, \mathbf{Z}\}$. Then, we compute $\mathbf{Z}_{[i,j]}$ via

$$625 \quad \mathbf{Z}_{[i,j]} = \sum_{k=1}^{\lceil p/4 \rceil} \mathbf{X}_{[i,k]} \mathbf{Y}_{[k,j]},$$

626 where we use (4.4) by initializing with $\mathbf{A}^{(1)} := \mathbf{X}_{[i,1]}$, $\mathbf{B}^{(1)} := \mathbf{Y}_{[1,j]}$, and $\mathbf{C}^{(1)} := \mathbf{0}_{4 \times 4}$ and setting
 627 $\mathbf{A}^{(k)} := \mathbf{X}_{[i,k]}$, $\mathbf{B}^{(k)} := \mathbf{Y}_{[k,j]}$, and $\mathbf{C}^{(k)} := \mathbf{D}^{(k-1)}$ for $k = 2 : \lceil p/4 \rceil$. By setting $\mathbf{C}^{(k)}, \mathbf{D}^{(k)} \in \mathbb{F}_{\text{fp32}}^{4 \times 4}$
 628 for $k > 1$ and only casting down at the end via $\mathbf{Z}_{[i,j]} = \text{fp16}(\mathbf{D}^{(\lceil p/4 \rceil)})$, we mostly employ fp32
 629 arithmetic for a mixed precision matrix product routine whose inputs and output are in fp16. For
 630 example, take $p = 8$. Then,

$$631 \quad \mathbf{D}^{(1)} = \text{fl}_{TC}(\mathbf{X}_{[i,1]} \mathbf{Y}_{[1,j]}), \quad \mathbf{D}^{(2)} = \text{fl}_{TC}(\mathbf{X}_{[i,2]} \mathbf{Y}_{[2,j]} + \mathbf{D}^{(1)}) \in \mathbb{F}_{\text{fp32}}^{4 \times 4}$$

$$632 \quad \mathbf{Z}_{[i,j]} = \text{castdown}(\mathbf{D}^{(2)}) \in \mathbb{F}_{\text{fp16}}^{4 \times 4}.$$

634 Adapting the rounding error analysis in [6] into this specific mixed precision matrix product setting
 635 yields the componentwise forward bound

$$636 \quad (4.5) \quad |\mathbf{Z} - \text{fl}(\mathbf{Z})| \leq \left(u^{(\text{fp16})} + \gamma_{p/4}^{(\text{fp32})} + u^{(\text{fp16})} \gamma_{p/4}^{(\text{fp32})} \right) |\mathbf{X}| |\mathbf{Y}|.$$

We denote BQR and TSQR computed via TensorCore bFMA's with `mpBQR3` and `mpTSQR3`, where the 3 represents the BLAS level-3 nature of this mixed precision setting.

4.1.1. BQR round down at block level: `mpBQR3`. Consider the input matrix, $\mathbf{A} \in \mathbb{F}_l^{m \times n}$, partitioned into N blocks of r columns, $\mathbf{A} = [\mathbf{C}_1 \cdots \mathbf{C}_N]$ as in [subsection 3.2](#). [Algorithm 7](#) shows a mixed precision variant of BQR that maximizes the use of bFMAs but uses high precision arithmetic for level-1 and 2 BLAS operations which are only a $\mathcal{O}(1/N)$ fraction of the total number of FLOPs. Each block is casted up to compute a high precision HQR and to form the WY representation. The WY representation is then casted down to low precision since the bFMAs require low precision inputs for matrix products, and the \mathbf{R} factor from the high precision HQR can be casted down to return a low precision \mathbf{R} factor at the very end. Since the cast down operations for the \mathbf{R} factor and the WY representations occur at every block, we can expect columnwise error bound for [alg. 7](#) to increase by approximately $Nu^{(l)}$ from the error bound for [alg. 5](#).

Algorithm 7: $\hat{\mathbf{Q}}_{mpBQR3}, \hat{\mathbf{R}}_{mpBQR3} \leftarrow \text{mpBQR3}(\mathbf{A}, r)$: Perform a mixed precision variant of BQR of low precision \mathbf{A} with column partitions of size r . $\hat{\mathbf{Q}}_{mpBQR3}, \hat{\mathbf{R}}_{mpBQR3}$, are returned in low precision. Operations in lines 7 and 10 require low precision inputs.

| | |
|---|--|
| <p>Input: \mathbf{A}, r.</p> <pre> 1 $N = \frac{n}{r}$ 2 for $k = 1 : N - 1$ do 3 $\mathbf{V}_k, \beta_k, \mathbf{C}_k \leftarrow \text{hhQR}(\text{castup}(\mathbf{C}_k))$ 4 $\mathbf{C}_k \leftarrow \text{castdown}(\mathbf{C}_k)$ 5 $\mathbf{W}_k \leftarrow \text{buildWY}(\mathbf{V}_k, \beta_k)$ 6 $[\mathbf{V}_k, \mathbf{W}_k] \leftarrow \text{castdown}([\mathbf{V}_k, \mathbf{W}_k])$ 7 $[\mathbf{C}_{k+1} \cdots \mathbf{C}_N] := \mathbf{V}_k (\mathbf{W}_k^\top [\mathbf{C}_{k+1} \cdots \mathbf{C}_N])$ 8 $\mathbf{Q} \leftarrow \mathbf{I}$ 9 for $k = N : -1 : 1$ do 10 $\mathbf{Q}[(k-1)r+1 : m, (k-1)r+1 : n] := \mathbf{W}_k (\mathbf{V}_k^\top \mathbf{Q}[(k-1)r+1 : m, (k-1)r+1 : n])$ 11 return \mathbf{Q}, \mathbf{A}</pre> | <p>Output: $\hat{\mathbf{Q}}_{mpBQR3}, \hat{\mathbf{R}}_{mpBQR3}$ /* Let $\mathbf{A} = [\mathbf{C}_1 \cdots \mathbf{C}_N]$. */</p> <p>/* Algorithm 3 in high precision. */ /* Builds \mathbf{R} factor in low precision. */ /* Algorithm 4 in high precision */ /* returned in low precision */ /* Build \mathbf{Q}: \mathbf{I}_m if full QR, and $\mathbf{I}_{m \times n}$ if thin QR. */</p> |
|---|--|

Since $\hat{\mathbf{W}}_k, \hat{\mathbf{Y}}_k$'s are computed with [alg. 4](#) in high precision then cast down, the new low precision WY update is $\hat{\mathbf{X}}_k^{(l)} = \mathbf{I} - \mathbf{I}^{(l)} \hat{\mathbf{W}}_k \mathbf{I}^{(l)} \hat{\mathbf{Y}}_k^{(T)}$. Consider applying $\hat{\mathbf{X}}_k^{(l)}$ to some matrix stored in low precision, \mathbf{B} using the TensorCore bFMAs. We analyze a single column $\mathbf{b}_j := \mathbf{B}[:, j] \in \mathbb{F}_l^{m-(k-1)r}$ even though this operation is done on \mathbf{B} as a whole. Let $\mathbf{I}^{(l)} \hat{\mathbf{W}}_k = (\mathbf{I} + \mathbf{E}_W) \hat{\mathbf{W}}_k$ and $\mathbf{I}^{(l)} \hat{\mathbf{Y}}_k = (\mathbf{I} + \mathbf{E}_Y) \hat{\mathbf{Y}}_k$, where $\mathbf{E}_W, \mathbf{E}_Y$ are diagonal and bounded componentwise by $u^{(l)}$. Then, the Frobenius norm error of forming $\hat{\mathbf{X}}_k^{(l)}$ is,

$$\begin{aligned}
\|\hat{\mathbf{X}}_k^{(l)} - \mathbf{X}_k\|_F &= \| -(\mathbf{I} + \mathbf{E}_W + \mathbf{E}_Y + \mathbf{E}_W \mathbf{E}_Y) \hat{\mathbf{W}}_k \hat{\mathbf{Y}}_k^\top + \mathbf{W}_k \mathbf{Y}_k^\top \|_F, \\
&\leq \left((1 + \gamma_2^{(l)} + (u^{(l)})^2) r \tilde{\gamma}_{m-(k-1)r}^{(h)} + \gamma_2^{(l)} + (u^{(l)})^2 \right) \|\mathbf{X}_k\|_F \\
&\leq \tilde{\gamma}_2^{(l)} + r \tilde{\gamma}_{m-(k-1)r}^{(h)} + r \tilde{\gamma}_2^{(l)} \tilde{\gamma}_{m-(k-1)r}^{(h)}.
\end{aligned}$$

Now, we consider the backward error of applying $\hat{\mathbf{X}}_k^{(l)}$ to \mathbf{b}_j with the bFMA matrix product error

bound from (4.5). The multiplication by $(\mathbf{I}^{(l)}\hat{\mathbf{Y}}_k)^\top$ yields backward error bounded by

$$\mathbf{fl}_{TC}((\mathbf{I}^{(l)}\hat{\mathbf{Y}}_k)^\top \mathbf{b}_j) = (\hat{\mathbf{Y}}_k + \Delta_{TC}\hat{\mathbf{Y}}_k)\mathbf{b}_j, \quad |\Delta_{TC}\hat{\mathbf{Y}}_k| \leq u^{(l)} + \gamma_{\frac{m-(k-1)}{4}}^{(h)} + u^{(l)}\gamma_{\frac{m-(k-1)}{4}}^{(h)}|\hat{\mathbf{Y}}_k||\mathbf{b}_j|,$$

and the subsequent multiplication by $(\mathbf{I}^{(l)}\hat{\mathbf{W}}_k)$ and subtraction from \mathbf{b}_j result in,

$$\begin{aligned} \mathbf{fl}_{TC}(\hat{\mathbf{X}}_k^{(l)}\mathbf{b}_j) &= (\hat{\mathbf{X}}_k^{(l)} + \Delta^{(l)}\mathbf{X}_k)\mathbf{b}_j, \\ |\Delta^{(l)}\mathbf{X}_k| &\leq \left(\gamma_2^{(l)} + \gamma_{1+\frac{m-(k-2)r}{4}}^{(h)} + \gamma_2^{(l)}\gamma_{1+\frac{m-(k-2)r}{4}}^{(h)} \right) \left(|\mathbf{b}_j| + |\mathbf{I}^{(l)}\hat{\mathbf{W}}_k||\mathbf{I}^{(l)}\hat{\mathbf{Y}}_k|^\top |\mathbf{b}_j| \right). \end{aligned}$$

Converting to a normwise error bound using the same logic from (3.9) and (3.10), we result in

$$(4.6) \quad \|\mathbf{fl}_{TC}(\hat{\mathbf{X}}_k^{(l)}\mathbf{b}_j) - \mathbf{X}_k\mathbf{b}_j\|_2 \leq (\tilde{\gamma}_2^{(l)} + r\tilde{\gamma}_{m-(k-1)r}^{(h)} + r\gamma_2^{(l)}\tilde{\gamma}_{m-(k-1)r}^{(h)})\|\mathbf{b}_j\|_2,$$

since the rounding errors from the bFMAs are small in comparison to the errors from casting down the WY representation built in high precision. The corresponding matrix error bound is

$$(4.7) \quad \|\mathbf{fl}_{TC}(\hat{\mathbf{X}}_k^{(l)}) - \mathbf{X}_k\|_F \leq \tilde{\gamma}_2^{(l)} + r\tilde{\gamma}_{m-(k-1)r}^{(h)} + r\gamma_2^{(l)}\tilde{\gamma}_{m-(k-1)r}^{(h)}.$$

We can finally compute the forward errors from implementing [alg. 7](#). Consider the j^{th} column of the \mathbf{Q} factor, which we denote with $\mathbf{q}_j := \hat{\mathbf{Q}}_{mpBQR3}[:, j]$, and let $k = \lfloor j/r \rfloor$. Invoking [Lemma 3.2](#) with error bounds for $\mathbf{fl}_{TC}(\hat{\mathbf{X}}_k^{(l)})$'s in (4.7) results in columnwise error,

$$(4.8) \quad \|\Delta\mathbf{q}_j\|_2 \leq -1 + \prod_{k'=1}^k (1 + \tilde{\gamma}_2^{(l)})(1 + r\tilde{\gamma}_{m-(k'-1)r}^{(h)})$$

$$(4.9) \quad \leq k\tilde{\gamma}_2^{(l)} + kr\tilde{\gamma}_m^{(h)} + k^2r\tilde{\gamma}_2^{(l)}\tilde{\gamma}_m^{(h)},$$

where $\Delta\mathbf{q}_j = (\mathbf{fl}_{TC}(\hat{\mathbf{X}}_1^{(l)}) \cdots \mathbf{fl}_{TC}(\hat{\mathbf{X}}_k^{(l)}) - \mathbf{X}_1 \cdots \mathbf{X}_k)\hat{\mathbf{e}}_j$. Summing over the columns to find a matrix norm error bound yields

$$(4.10) \quad \|\hat{\mathbf{Q}}_{mpBQR} - \mathbf{Q}\|_F \leq n^{1/2} \left(\tilde{\gamma}_N^{(l)} + n\tilde{\gamma}_m^{(h)} \right),$$

where the summation of the third term in (4.9) is swept under the tilde notation in $n^{1/2}\tilde{\gamma}_N^{(l)}$. This bound shows that [alg. 7](#) only adds $n^{1/2}\tilde{\gamma}_N^{(l)}$ order errors to the bounds in (3.22). Using that $u^{(l)} = M_{l,h}u^{(h)}$, this increase corresponds to a multiplicative factor shown below,

$$(4.11) \quad n^{1/2}\tilde{\gamma}_N^{(l)} + n^{(3/2)}\tilde{\gamma}_m^{(h)} \approx \left(1 + \frac{M_{l,h}}{rm} \right) n^{(3/2)}\tilde{\gamma}_m^{(h)}.$$

Therefore, the loss in accuracy due to mixed precision computing is relatively small when the disparity in precision ($M_{l,h}$) is small in comparison to the block size, mr . However, as r grows large, $N = n/r$ decreases which then reduces the portion of `mpBQR3` performed using level-3 BLAS operations and increases the size of high precision HQR being performed at each block. Whether this loss in accuracy in the worst-case scenario is worth the speed-ups from using mixed precision hardware is an open question that can be tackled in future research. Our analysis shows that the block size r , the dimension of the input matrix m, n , and hardware specificities will be contributing factors.

4.1.2. TSQR round down at block level: mpTSQR3. Unlike BQR which is rich in level-3 BLAS operations, the variant of TSQR in [alg. 6](#) uses none. Therefore, we modify [alg. 6](#) by replacing all instances of `hh_mult` with level-3 BLAS operations. We omit presenting the exact algorithm for mixed precision variant of TSQR in this paper, but consider computing the HQR of each block in high precision and build and store the WY representation of the HH transformations in low precision as we did in lines (3-6) of [alg. 7](#). The low precision WY representation is then applied with TensorCore bFMAs when building the \mathbf{Q} factor (lines 11-16 of [alg. 6](#)).

Rounding Error analysis. The analysis in [\[21\]](#) shows that each column of \mathbf{Q} is transformed by n HH transformations of length $2n$ from levels $L : -1 : 1$, and another set of n HH transformations of length $m2^{-L}$ at level 0. Let us represent the WY representation at the j^{th} block of level i and its bFMA counterpart as $\mathbf{X}_j^{(i)}$ and $\text{fl}_{TC}(\hat{\mathbf{X}}_j^{(i)})$. Then, we can use [\(4.7\)](#) to form backward error

$$(4.12) \quad \|\text{fl}_{TC}(\hat{\mathbf{X}}_j^{(i)}) - \mathbf{X}_j^{(i)}\|_F \leq \tilde{\gamma}_2^{(l)} + n\tilde{\gamma}_{m'}^{(h)} + n\tilde{\gamma}_2^{(l)}\tilde{\gamma}_{m'}^{(h)}, \quad m' = \begin{cases} m2^{-L}, & i = 0 \\ 2n, & i = 1 : L \end{cases}.$$

We can now modify the analysis in [\[21\]](#) by replacing $n\tilde{\gamma}_{m2^{-L}}$ and $n\tilde{\gamma}_{2n}$ with

$$(1 + \tilde{\gamma}_2^{(l)})(1 + n\tilde{\gamma}_{m2^{-L}}^{(h)}) - 1, \quad \text{and} \quad (1 + \tilde{\gamma}_2^{(l)})(1 + n\tilde{\gamma}_{2n}^{(h)}) - 1,$$

and apply [Lemma 3.2](#). Then, the factors formed by mpTSQR3 are denoted by $\hat{\mathbf{R}}_{mpTSQR3}$, $\hat{\mathbf{Q}}_{mpTSQR3}$ and the error bounds for the j^{th} column of the triangular factor and the orthogonal factor are

$$\|(\hat{\mathbf{R}}_{mpTSQR3} - \mathbf{R})[:, j]\|_2 \leq \tilde{\gamma}_{L+1}^{(l)} + n \left(L\tilde{\gamma}_{2n}^{(h)} + \tilde{\gamma}_{m2^{-L}}^{(h)} \right) \|\mathbf{A}[:, j]\|_2,$$

$$\|\hat{\mathbf{Q}}_{mpTSQR3} - \mathbf{Q}\|_F \leq n^{1/2}\tilde{\gamma}_{L+1}^{(l)} + n^{3/2} \left(L\tilde{\gamma}_{2n}^{(h)} + \tilde{\gamma}_{m2^{-L}}^{(h)} \right).$$

Converting the low precision rounding errors as a fraction of the TSQR error bound in [\(3.24\)](#) to quantify the impact of modifying [alg. 6](#) to utilize bFMAs yields

$$(4.13) \quad n^{1/2}\tilde{\gamma}_{L+1}^{(l)} + n^{3/2} \left(L\tilde{\gamma}_{2n}^{(h)} + \tilde{\gamma}_{m2^{-L}}^{(h)} \right) = \left(1 + \frac{M_{l,h}(L+1)}{n(2nL + m2^{-L})} \right) n^{3/2} \left(L\tilde{\gamma}_{2n}^{(h)} + \tilde{\gamma}_{m2^{-L}}^{(h)} \right).$$

Like in [\(4.11\)](#), the disparity in the two precisions, $M_{l,h}$ is compared against the original matrix size m, n and the block size specifications derived from L . Let us consider the shallowest, middle, and the deepest levels of TSQR that are possible given some matrix in $\mathbb{R}^{m \times n}$. All three cases in [Table 4](#) show that mpTSQR3 on sufficiently large matrices may yield errors closer to the high precision implementation, and the optimal choice for L depends on m, n .

| Number of levels, L | 1 | $\frac{1}{2} \log_2(m/n)$ | $-1 + \log_2(m/n)$ |
|--------------------------------|-----------------|--|--------------------|
| $\frac{(L+1)}{n(2nL+m2^{-L})}$ | $1/(n^2 + m/4)$ | $1/\left(2n^2 + \frac{m^{1/2}n^{3/2}}{\log_2(m/n)}\right)$ | $1/(2n^2)$ |

TABLE 4
Error bounds for $\|\Delta\mathbf{Q}_{mpTSQR3}\|_F$ for varying L 's.

4.2. Round down at inner product: level-2 BLAS mixed precision setting. While the previous section discussed blocked variants of HQR that can be easily adapted for the mixed precision setting specific to TensorCore bFMA's, we want to provide a more general mixed precision environment in this section. Recall that HQR, BQR, and TSQR all rely on HH transformations

in one way or another, and implementations of HH transformations are expressed by (3.8). This implementation capitalizes on the rank-1 update structure of HH transformations where the predominant share of FLOPs is spent on an inner product, and computing the HH vector and constant also rely heavily on inner products. Therefore, nearly all of the computational tasks for algs. 3, 5 and 6 are attributed to the inner product, which is important in other linear algebra tools such as projections, matrix-vector, and matrix-matrix multiply. Consequently, we return to MP Setting 2.3, where every inner product is cast down to the lower precision as shown in (2.10). We denote HQR, BQR, and TSQR computed with MP Setting 2.3 with mpHQR2, mpBQR2, and mpTSQR2, where the 2 represents the mixed precision procedure computed at a level-2 BLAS operation.

4.2.1. HQR round down at inner product: mpHQR2. Consider forming a HH transformation that zeros out $\mathbf{x} \in \mathbb{R}^m$ below the i^{th} element. We need to compute σ , β , $\hat{\mathbf{v}}_1$, and \mathbf{v} as defined in subsection 3.1,

$$(4.14) \quad \text{fl}(\sigma) = \text{fl}(-\text{sign}(\mathbf{x}[1])\|\mathbf{x}\|_2) = \sigma + \Delta\sigma, \quad |\Delta\sigma| \leq \left(\gamma_2^{(l)} + \gamma_m^{(h)} + \gamma_2^{(l)}\gamma_m^{(h)}\right)|\sigma|,$$

$$(4.15) \quad \text{fl}(\mathbf{v}'[1]) = \mathbf{v}'[1] + \Delta\mathbf{v}'[1] = (1 + \delta^{(l)})(\mathbf{x}[1] - \sigma - \Delta\sigma), \quad |\Delta\mathbf{v}'[1]| \leq (\gamma_3^{(l)} + \tilde{\gamma}_m^{(h)})|\mathbf{v}'[1]|$$

$$(4.16) \quad \text{fl}(\beta) = \beta + \Delta\beta = (1 + \delta^{(l)})(-\mathbf{v}'[1]/\hat{\sigma}), \quad |\Delta\beta| \leq (\gamma_8^{(l)} + \tilde{\gamma}_m^{(h)})|\beta|,$$

$$(4.17) \quad \text{fl}(\mathbf{v}[j]) = \mathbf{v}[j] + \Delta\mathbf{v}[j] \text{ where } |\Delta\mathbf{v}[j]| \leq (\gamma_7^{(l)} + \tilde{\gamma}_m^{(h)})|\mathbf{v}_j|, j = 2 : m - i + 1.$$

These bounds on $\Delta\sigma$, $\Delta\mathbf{v}'[1]$, $\Delta\beta$, and $\Delta\mathbf{v}[j]$ are computed by using the rules from Lemma 2.4 on the analysis shown in subsection 3.1. Using these, we can formulate the mixed precision version of (3.9) where $\hat{\mathbf{y}} = \text{fl}(\mathbf{P}_\mathbf{v}\mathbf{x}) \in \mathbb{R}^m$ is implemented via (3.8). Note that the inner product $\hat{\mathbf{v}}^\top \mathbf{x}$ via MP Setting 2.3, and all other operations are done in the lower precision. Then, the transformed vector is bounded by

$$(4.18) \quad \hat{\mathbf{y}} = \mathbf{y} + \Delta\mathbf{y}, \quad \|\Delta\mathbf{y}\|_2 \leq (\gamma_{25}^{(l)} + \tilde{\gamma}_m^{(h)})\|\mathbf{y}\|_2.$$

Thus, a backward error can be formed using $\Delta\mathbf{P}_\mathbf{v} = \Delta\mathbf{y}\mathbf{x}^\top / \|\mathbf{x}\|_2^2$,

$$(4.19) \quad \hat{\mathbf{y}} = (\mathbf{P}_\mathbf{v} + \Delta\mathbf{P}_\mathbf{v})\mathbf{x}, \quad \|\Delta\mathbf{P}_\mathbf{v}\|_F \leq (\gamma_{25}^{(l)} + \tilde{\gamma}_m^{(h)}).$$

Now, we form the error bounds for applying n HH transformations to \mathbf{x} using Lemma 3.2,

$$(4.20) \quad \hat{\mathbf{z}} = \text{fl}(\mathbf{P}_1 \cdots \mathbf{P}_n \mathbf{x}) = \mathbf{Q}(\mathbf{x} + \Delta\mathbf{x}) = (\mathbf{Q} + \Delta\mathbf{Q})\mathbf{x},$$

$$(4.21) \quad \|\Delta\mathbf{y}\|_2 \leq (\tilde{\gamma}_n^{(l)} + n\tilde{\gamma}_m^{(h)})\|\mathbf{x}\|_2, \quad \|\Delta\mathbf{Q}\|_F \leq (\tilde{\gamma}_n^{(l)} + n\tilde{\gamma}_m^{(h)}).$$

Note that we use the $\tilde{\gamma}^{(l)}$ notation, where the small integer c is now required to be $\mathcal{O}(25)$. The analogous mixed precision QR factorization error bounds are shown in Theorem 4.1.

THEOREM 4.1. *Let $\mathbf{A} \in \mathbb{R}^{m \times n}$ with $m \geq n$ have full rank, n . Let $\hat{\mathbf{Q}}_{mpHQR2} \in \mathbb{R}^{m \times n}$ and $\hat{\mathbf{R}} \in \mathbb{R}_{mpHQR2}^{n \times n}$ be the thin QR factors of \mathbf{A} obtained via alg. 3 with mixed precision FLOPs where inner products are computed in precision h then cast down. All other operations are carried out in precision l . Then,*

$$(4.22) \quad \|\Delta\mathbf{R}_{mpHQR2}[:, j]\|_2 \leq (\tilde{\gamma}_n^{(l)} + n\tilde{\gamma}_m^{(h)})\|\mathbf{A}[:, j]\|_2, \quad \|\Delta\mathbf{R}_{mpHQR2}\|_F \leq (\tilde{\gamma}_n^{(l)} + n\tilde{\gamma}_m^{(h)})\|\mathbf{A}\|_F$$

$$(4.23) \quad \|\Delta\mathbf{Q}[:, j]_{mpHQR2}\|_2 \leq (\tilde{\gamma}_n^{(l)} + n\tilde{\gamma}_m^{(h)}), \quad \|\Delta\mathbf{Q}_{mpHQR2}\|_F \leq n^{1/2}(\tilde{\gamma}_n^{(l)} + n\tilde{\gamma}_m^{(h)}).$$

Unsurprisingly, the inner product mixed precision setting yields higher error bounds as it uses more low precision arithmetic than the settings described in subsection 4.1. In the next sections we analyze using mpHQR2 instead of HQR within algs. 5 and 6.

4.2.2. BQR round down at inner product: mpBQR2. Now, we analyze [alg. 5](#) implemented with [MP Setting 2.3](#). At the k^{th} block, we first apply the mixed precision HQR summarized in [Theorem 4.1](#). Next, we construct the WY representation, where we can now use [\(4.18\)](#) and [\(4.19\)](#) and [Lemma 3.2](#) to form

$$(4.24) \quad \|\hat{\mathbf{X}}_k^{(l)} - \mathbf{X}_k\|_F = \|(\hat{\mathbf{P}}_k^{(1)} \cdots \hat{\mathbf{P}}_k^{(r)}) - (\mathbf{P}_k^{(1)} \cdots \mathbf{P}_k^{(r)})\|_F \leq \tilde{\gamma}_r^{(l)} + r\tilde{\gamma}_m^{(h)}.$$

Then, the 2-norm bound for the j^{th} column of the \mathbf{R} factor and the Frobenius norm bound for the orthogonal factor resulting from mpBQR2 are

$$(4.25) \quad \|\hat{\mathbf{R}}_{mpBQR2}[:, j]\|_2 = \|\hat{\mathbf{X}}_1 \cdots \hat{\mathbf{X}}_N \mathbf{A}[:, j]\|_2 \leq (N\tilde{\gamma}_r^{(l)} + n\tilde{\gamma}_m^{(h)}) \|\mathbf{A}[:, j]\|_2,$$

$$(4.26) \quad \|\hat{\mathbf{Q}}_{mpBQR2}\|_F \leq n^{1/2} (N\tilde{\gamma}_r^{(l)} + n\tilde{\gamma}_m^{(h)}) \approx \left(1 + \frac{M_{l,h}}{m}\right) n^{3/2} \tilde{\gamma}_m^{(h)}.$$

Note that this error bound is of the same order as the error bound for mpHQR2, shown in [\(4.23\)](#). The corresponding error bound for mpBQR3 of [section 4.1.1](#) yielded low precision errors r times smaller than that from using [MP Setting 2.3](#) inner products, an unsurprising result as intermediate results are cast down more often in mpBQR2. Furthermore, the $\tilde{\gamma}^{(l)}$ in this section requires $c = \mathcal{O}(25)$, whereas the same notation in [section 4.1.1](#) assumes c to be a *small* positive integer. Therefore, the numerical stability of mpBQR2 is guaranteed at smaller matrix sizes than the numerical stability of mpBQR3 and BQR in high precision. While it is technically possible that the low precision errors introduced from utilizing [MP Setting 2.3](#) do not dominate the errors incurred in mpBQR2 and mpHQR2 when $m \gg M_{l,h}$ and can result in accuracy comparable to that of mpBQR3 and high precision BQR, our numerical results in [section 5](#) show that mpHQR2 is already unstable at $m \approx M_{l,h}$.

4.2.3. TSQR round down at inner product: mpTSQR2. Finally, we consider using [MP Setting 2.3](#) in [alg. 6](#). This corresponds to replacing every instance of $n\tilde{\gamma}_{m'}^{(h)}$ for $m' \in \{2n, m2^{-L}\}$ in [Theorem 3.7](#) with $\tilde{\gamma}_n^{(l)} + n\tilde{\gamma}_{m'}^{(h)}$. We first consider the norm errors for the j^{th} column of the \mathbf{Q} factor computed by this mixed precision variant of [alg. 6](#),

$$(4.27) \quad \|\hat{\mathbf{Q}}_{mpTSQR2}[:, j] - \mathbf{Q}[:, j]\|_2 \leq (L+1)\tilde{\gamma}_n^{(l)} + n(\tilde{\gamma}_{m2^{-L}}^{(h)} + L\tilde{\gamma}_{2n}^{(h)}).$$

Then, the matrix norm error bound is

$$(4.28) \quad \|\hat{\mathbf{Q}}_{mpTSQR2} - \mathbf{Q}\|_F \leq n^{1/2} (L+1)\tilde{\gamma}_n^{(l)} + n^{3/2} (\tilde{\gamma}_{m2^{-L}}^{(h)} + L\tilde{\gamma}_{2n}^{(h)})$$

$$(4.29) \quad \approx \left(1 + \frac{M_{l,h}L}{m2^{-L} + 2Ln}\right) n^{3/2} (\tilde{\gamma}_{m2^{-L}}^{(h)} + L\tilde{\gamma}_{2n}^{(h)}),$$

and contributes larger low precision rounding errors than in [\(4.13\)](#). If the mpTSQR2 error bound were to outperform that of mpHQR2, we now need integers $m, n > 0$, and $L \geq 0$ that satisfy

$$1 \gg n^{1/2} (\tilde{\gamma}_n^{(l)} + n\tilde{\gamma}_m^{(h)}) \gg n^{1/2} ((L+1)\tilde{\gamma}_n^{(l)} + n(\tilde{\gamma}_{m2^{-L}}^{(h)} + L\tilde{\gamma}_{2n}^{(h)})).$$

In contrast to the analysis for uniform precision settings, large L values do not necessarily reduce the error bounds of TSQR. While large L can imply $m \gg m2^{-L} + 2Ln$, it does not always lead to $d \gg d_1 + Ld_2$. Although the theoretical error bounds do not give a clear indication of the worst-case performances of HQR and TSQR in mixed-precision settings, TSQR outperformed HQR on ill-conditioned matrices within our numerical simulations.

These experiments are discussed in detail in the next section.

5. Numerical Experiments. We conducted several numerical experiments to confirm the validity of the error bounds formed in section 4. First, we tested algs. 3 and 5 to 7, mpHQR2, mpBQR2, and mpTSQR2 for varying matrix sizes. Then, we compared the performance of mpHQR2 and mpTSQR2, and lastly, tested varying block sizes in alg. 7 for a fixed matrix size. We used Julia, a programming language which allows fp16 storage and `castup` and `castdown` operations between types in fp16, fp32, fp64, but no built-in fp16 arithmetic. Therefore, we relied on using alg. 1 for $f \in \text{OP} \cup \{\text{dot_product}\}$ to simulate MP Setting 2.3 and TensorCore bFMAs.

In sections 3 and 4, we gave the forward error bounds for \mathbf{R} and \mathbf{Q} separately. Since our numerical experiments instead measure a backward error, $\|\hat{\mathbf{Q}}\hat{\mathbf{R}} - \mathbf{A}\|_F$, and an orthogonal error, $\|\hat{\mathbf{Q}}^\top \hat{\mathbf{Q}} - \mathbf{I}\|_2$, we show how to convert general forward errors into those computed quantities. Given $\|(\hat{\mathbf{R}} - \mathbf{R})[:, j]\|_2 \leq \epsilon_R \|\mathbf{A}[:, j]\|_2$ and $\|\hat{\mathbf{Q}} - \mathbf{Q}\|_F \leq \epsilon_Q$,

$$(5.1) \quad \|(\hat{\mathbf{Q}}\hat{\mathbf{R}} - \mathbf{A})[:, j]\|_2 \leq (\epsilon_R + \epsilon_Q + \epsilon_R \epsilon_Q) \|\mathbf{A}[:, j]\|_2, \quad j = 1 : n, \quad \text{see [15]},$$

$$(5.2) \quad \|\hat{\mathbf{Q}}\hat{\mathbf{R}} - \mathbf{A}\|_F \leq n^{1/2}(\epsilon_R + \epsilon_Q + \epsilon_R \epsilon_Q) \|\mathbf{A}\|_F,$$

$$(5.3) \quad \|\hat{\mathbf{Q}}^\top \hat{\mathbf{Q}} - \mathbf{I}\|_2 \leq \|\hat{\mathbf{Q}}^\top \hat{\mathbf{Q}} - \mathbf{I}\|_F \simeq 2\epsilon_Q, \quad \text{see [21]}.$$

The left plot of Figure 2 shows the backward error for HQR, BQR, TSQR, and their mixed

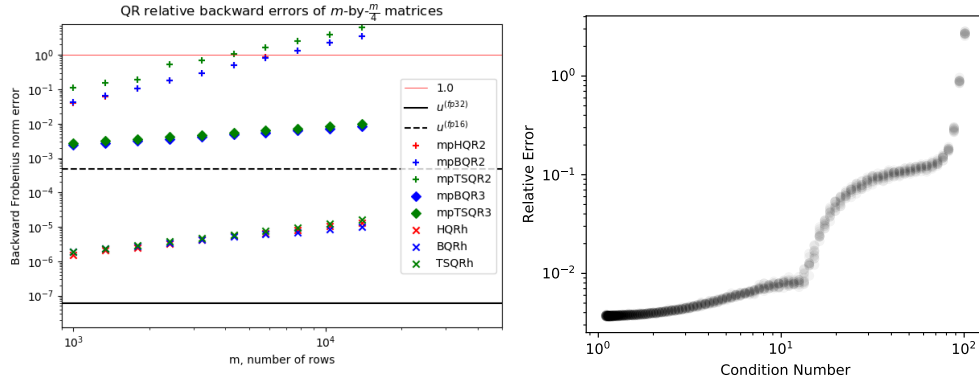


FIG. 2. Left plot: Relative backward error of all HH QR factorization algorithms discussed in sections 3 and 4 with varying matrix sizes. Right plot: mpHQR2 errors for 4000-by-100 matrices with varying condition numbers.

precision variants. We increased the number of rows m from 1000 to 13949, while keeping $n = m/4$, $r = n/4$, and $L = 2$ and condition number at 1000 by generating $\mathbf{A} = \text{castdown}(\mathbf{Q}_1 \mathbf{D} \mathbf{Q}_2)$ where $\mathbf{Q}_1 \in \mathbb{F}_h^{m \times n}$, $\mathbf{Q}_2 \in \mathbb{F}_h^{n \times n}$ are orthogonal and $\mathbf{D} = \text{Diagonal}(\{\log_{10}(0), \dots, \log_{10}(-3)\}) \in \mathbb{F}_h^{n \times n}$. The three clusters each correspond to: top, MP Setting 2.3; middle, TensorCore bFMAs; and bottom, uniform precision implementations in fp32. The high precision and bFMA implementations scale similarly to each other when increasing the matrix size, whereas the MP Setting 2.3 variants grow unstable more quickly. In addition, while HQR, BQR, and TSQR perform similarly in high precision and when using bFMAs, mpTSQR2 is less accurate by a quarter to a half order of magnitude in comparison to mpBQR2 and mpHQR2. The specifications for $m, n, L, M_{l,h}$ for this experiment derive the upper bound for $\|\Delta \mathbf{Q}_{mpTSQR2}\|_F$, (4.29), to be larger than that of $\|\Delta \mathbf{Q}_{mpHQR2}\|_F$, (4.23). However, a more careful comparison of mpHQR2 and mpTSQR2 show that there exists a regime where mpTSQR2 can outperform mpHQR2.

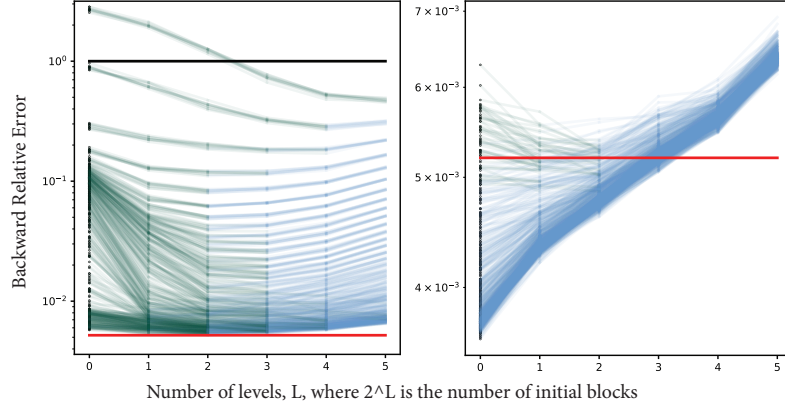


FIG. 3. Left plot shows the relative error of QR factorization for matrices with condition numbers ranging from 5.3 to 101, and the right plot shows the errors for matrices with condition numbers ranging from 1.1 to 5.3.

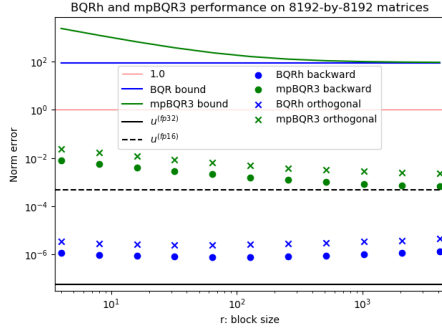


FIG. 4. Relative backward error of mpBQR3 for 8192-by-8192 matrices are shown with block size r ranging from 4 to 4096.

$\|\hat{\mathbf{Q}}\hat{\mathbf{R}} - \mathbf{A}\|_F / \|\mathbf{A}\|_F$, was computed by casting up $\hat{\mathbf{Q}}$, $\hat{\mathbf{R}}$, and \mathbf{A} to fp64 to compute the Frobenius norms. Plugging in $m = 4000$, $n = 100$, $u^{(l)} = u^{(fp16)}$, $u^{(h)} = u^{(fp32)}$, and $c = 1$ (for $\tilde{\gamma}$) into the error bounds for mpHQR2 combined with (5.2) and (5.3) are approximately 1.179 and 1.146. These error bounds are *relative* and these worst-case bounds do not guarantee errors below 100%. The TSQR bounds for the same parameters for $L = 1 : 5$ are even larger, which indicates that stability is not guaranteed. The right plot of Figure 3 shows the backward errors of mpHQR2 increasing as the theoretical condition numbers of the generated random matrices increase, and these errors correspond to the error data on the vertical axis, $L = 0$, of Figure 3. In addition to the errors from mpHQR2, Figure 3 shows the errors from mpTSQR2s of levels varying from $L = 1$ to $L = 5$, where each line represents the errors of HQR and variants of TSQR calculated from the same random test matrix. Figure 3 reveals two different trends for the errors as we deepen the complexity of the QR algorithm from mpHQR2 to mpTSQR2 with $L = 5$. One trend occurs for matrices with smaller condition numbers, where mpHQR2 is stable, but mpTSQR2 with higher levels yield larger errors. Another trend occurs for matrices with higher condition numbers, where single-level and 2-level mpTSQR2

yield smaller errors than `mpHQR2`. In these cases, errors from `mpTSQR2` with 3 or more levels are similar to or worse than their 2-level variants, but generally do not exceed those of `mpHQR2` most of the times. These results suggests that TSQR can outperform HQR even in mixed precision settings, and particularly when HQR is unstable due to larger condition numbers. Although this experiment focused on condition numbers, identifying other properties that point to better performance of TSQR than HQR can further broaden the potential use of mixed precision TSQR in applications.

Finally, we discuss the last experiment which varied the block sizes for `mpBQR3`. Figure 4 shows the error bounds and the computed value for the backward error for fp32 BQR and `mpBQR3` for $m = n = 8193$ and varying r . The test matrices were sampled from $N(0, 1)$, and their large size immediately pushes both error bounds above 1 and numerical stability is not guaranteed. However, the high precision implementation yields backward error close to $u^{(fp32)}$ and `mpBQR3` yields errors near $u^{(fp16)}$ that follows the downward trend suggested by (4.11). The rightmost data for `mpBQR3` (corresponds to $r = n/2$), is still between 2 and 3 orders of magnitude higher than its high precision variant. There exist applications that are robust to QR factorization errors and could benefit from speed-ups of using bFMAs.

In conclusion, most of the experiments display the trends that error bounds in sections 3 and 4 suggest, and bFMA variants perform in between the high precision and MP Setting 2.3 variants as expected. Also, a special case is shown that demonstrate `mpTSQR2` can outperform `mpHQR2` despite having higher error bounds. Although further studies with larger problem sizes and timings would be beneficial in developing an `mpBQR3` with the optimal block size, r , our experiments confirm the intuition built from the error analysis in section 4.

6. Conclusion. The development of GPUs that optimize low precision floating point arithmetic have accelerated the interest in half and mixed precision algorithms that naturally reduces the bandwidth and storage needs. Loss in precision, stability, and representable range offset for those advantages, but these shortcomings may have little to no impact in some applications. It may even be possible to navigate around those drawbacks with algorithmic design.

We present the algorithm and standard error analysis of HQR and its blocked variants (BQR and TSQR), modify the algorithms to support two mixed precision settings, and performed error analysis that accurately bound the mixed precision versions. One mixed precision setting is that of NVIDIA’s TensorCore bFMAs, and the other is an ad hoc setting that mimics the bFMAs at the level of inner products. These two are presented to offer mixed precision arithmetic at both level-2 and 3 BLAS operations and can be applied to other linear algebra tools as well. The new error bounds more accurately describe how rounding errors are accumulated in mixed precision settings. We also found that TSQR can outperform HQR under MP Setting 2.3 for ill-conditioned, extremely overdetermined cases, which suggests that some algorithms are more robust against lower precision arithmetic. Future work is needed to test larger problem sizes with timed experiments to compare the loss in accuracy with the benefits of speed ups and explore other divide-and-conquer methods like TSQR that can harness parallel capabilities of GPUs while withstanding lower precisions.

REFERENCES

- [1] A. ABDEFATTAH, S. TOMOV, AND J. DONGARRA, *Fast batched matrix multiplication for small sizes using half-precision arithmetic on GPUs*, in 2019 IEEE International Parallel and Distributed Processing Symposium (IPDPS), May 2019, pp. 111–122, <https://doi.org/10.1109/IPDPS.2019.00022>.
- [2] E. ANDERSON, Z. BAI, C. BISCHOF, L. S. BLACKFORD, J. DEMMEL, J. J. DONGARRA, J. DU CROZ, S. HAMMARLING, A. GREENBAUM, A. MCKENNEY, AND D. SORENSSEN, *LAPACK Users’ Guide (Third Ed.)*, Society for Industrial and Applied Mathematics, Philadelphia, PA, USA, 1999; also available online from

- <http://www.netlib.org>.
- [3] J. APPELYARD AND S. YOKIM, *Programming Tensor Cores in CUDA 9*, 2017, <https://devblogs.nvidia.com/programming-tensor-cores-cuda-9/> (accessed 2018-07-30).
 - [4] G. BALLARD, J. W. DEMMEL, L. GRIGORI, M. JACQUELIN, H. DIEP NGUYEN, AND E. SOLOMONIK, *Reconstructing Householder vectors from tall-skinny QR*, vol. 85, 05 2014, pp. 1159–1170, <https://doi.org/10.1109/IPDPS.2014.120>.
 - [5] C. BISCHOF AND C. VAN LOAN, *The WY Representation for Products of Householder Matrices*, SIAM Journal on Scientific and Statistical Computing, 8 (1987), pp. s2–s13, <https://doi.org/10.1137/0908009>.
 - [6] P. BLANCHARD, N. J. HIGHAM, F. LOPEZ, T. MARY, AND S. PRANESH, *Mixed Precision Block Fused Multiply-Add : Error Analysis and Application to GPU Tensor Cores*, (2019).
 - [7] M. COURBARIAUX, Y. BENGIO, AND J.-P. DAVID, *Training deep neural networks with low precision multiplications*, arXiv preprint, arXiv:1412.7024, (2014).
 - [8] M. COURBARIAUX, J.-P. DAVID, AND Y. BENGIO, *Low precision storage for deep learning*, arXiv preprint arXiv:1412.7024, (2014).
 - [9] J. DEMMEL, I. DUMITRIU, AND O. HOLTZ, *Fast linear algebra is stable*, Numerische Mathematik, 108 (2007), pp. 59–91, <https://doi.org/10.1007/s00211-007-0114-x>, <https://arxiv.org/abs/0612264>.
 - [10] J. DEMMEL, L. GRIGORI, M. HOEMMEN, AND J. LANGOU, *Communication-optimal parallel and sequential QR and LU factorizations*, SIAM Journal on Scientific Computing, 34 (2012), <https://doi.org/10.1137/080731992>, <https://arxiv.org/abs/0808.2664>.
 - [11] M. FAGAN, J. SCHLACHTER, K. YOSHII, S. LEYFFER, K. PALEM, M. SNIR, S. M. WILD, AND C. ENZ, *Overcoming the power wall by exploiting inexactness and emerging COTS architectural features: Trading precision for improving application quality*, in 2016 29th IEEE International System-on-Chip Conference (SOCC), Sep. 2016, pp. 241–246, <https://doi.org/10.1109/SOCC.2016.7905477>.
 - [12] G. H. GOLUB AND C. F. VAN LOAN, *Matrix computations*, JHU press, 4 ed., 2013.
 - [13] A. HAIDAR, A. ABDELFAH, M. ZOUNON, P. WU, S. PRANESH, S. TOMOV, AND J. DONGARRA, *The Design of Fast and Energy-Efficient Linear Solvers: On the Potential of Half-Precision Arithmetic and Iterative Refinement Techniques*, June 2018, pp. 586–600, https://doi.org/10.1007/978-3-319-93698-7_45.
 - [14] A. HAIDAR, S. TOMOV, J. DONGARRA, AND N. J. HIGHAM, *Harnessing GPU tensor cores for fast fp16 arithmetic to speed up mixed-precision iterative refinement solvers*, in Proceedings of the International Conference for High Performance Computing, Networking, Storage, and Analysis, SC '18, Piscataway, NJ, USA, 2018, IEEE Press, pp. 47:1–47:11, <https://doi.org/10.1109/SC.2018.00050>, <https://doi.org/10.1109/SC.2018.00050>.
 - [15] N. J. HIGHAM, *Accuracy and Stability of Numerical Methods*, 2002, <https://doi.org/10.2307/2669725>.
 - [16] N. J. HIGHAM AND T. MARY, *A New Approach to Probabilistic Rounding Error Analysis*, SIAM Journal on Scientific Computing, 41 (2019), pp. A2815–A2835, <https://doi.org/10.1137/18M1226312>, <https://epubs.siam.org/doi/10.1137/18M1226312>.
 - [17] N. J. HIGHAM AND S. PRANESH, *Simulating Low Precision Floating-Point Arithmetic*, SIAM Journal on Scientific Computing, 41 (2019), pp. C585–C602, <https://doi.org/10.1137/19M1251308>, <https://epubs.siam.org/doi/10.1137/19M1251308>.
 - [18] A. S. HOUSEHOLDER, *Unitary triangularization of a nonsymmetric matrix*, Journal of the ACM (JACM), 5 (1958), pp. 339–342.
 - [19] I. C. F. IPSEN AND H. ZHOU, *Probabilistic Error Analysis for Inner Products*, (2019), <http://arxiv.org/abs/1906.10465>, <https://arxiv.org/abs/1906.10465>.
 - [20] P. MICKEVICIUS, S. NARANG, J. ALBEN, G. DIAMOS, E. ELSSEN, D. GARCIA, B. GINSBURG, M. HOUSTON, O. KUCHAIEV, G. VENKATESH, AND H. WU, *Mixed precision training*, in International Conference on Learning Representations, 2018, <https://openreview.net/forum?id=r1gs9JgRZ>.
 - [21] D. MORI, Y. YAMAMOTO, AND S. L. ZHANG, *Backward error analysis of the AllReduce algorithm for householder QR decomposition*, Japan Journal of Industrial and Applied Mathematics, 29 (2012), pp. 111–130, <https://doi.org/10.1007/s13160-011-0053-x>.
 - [22] R. SCHREIBER AND C. VAN LOAN, *A Storage-Efficient \$WY\$ Representation for Products of Householder Transformations*, SIAM Journal on Scientific and Statistical Computing, 10 (1989), pp. 53–57, <https://doi.org/10.1137/0910005>.
 - [23] G. TAGLIAVINI, S. MACH, D. ROSSI, A. MARONGIU, AND L. BENIN, *A transprecision floating-point platform for ultra-low power computing*, in 2018 Design, Automation Test in Europe Conference Exhibition (DATE), March 2018, pp. 1051–1056, <https://doi.org/10.23919/DATE.2018.8342167>.
 - [24] U. VON LUXBURG, *A tutorial on spectral clustering*, Statistics and Computing, 17 (2007), pp. 395–416, <https://doi.org/10.1007/s11222-007-9033-z>, <https://doi.org/10.1007/s11222-007-9033-z>.